Assimilation of snow covered area into a hydrologic model

A thesis
submitted in partial fulfilment
of the requirements for the Degree
of

Master of Science in Geography

in the

University of Canterbury

by

Einar Örn Hreinsson

University of Canterbury

2008

Contents

List of Figures

List of Tables

Acknowledgement

I would like to thank my supervisors, Dr. Martyn P. Clark and Dr. Ian F. Owens, for their valuable help during this study. I would also like to thank NIWA for supplying the hydrologic model and necessary data and Pascal J. Sirguey for supplying the remotely sensed images. Steven Sykes made it possible for me to use Tornado for running the model. I also have to mention Tim Kerr, Dr. Jordy Hendrikx, Justin Harrison, Nick Key and others who assisted me at some stage in this study. And finally all the people I joined in a number of fieldtrips into the Jollie.

The dataset used in this study MODIS *Subpixel Snow Fraction of the Upper Waitaki Catchment, New Zealand*, V1-0, was processed by Pascal J. Sirguey (2007), GLIMS NZ Office, School of Surveying, University of Otago, Dunedin, New Zealand.

Abstract

Accurate knowledge of water content in seasonal snow can be helpful for water resource management. In this study, a distributed temperature index snow model based on temperature and precipitation as forcing data, is used to estimate snow storage in the Jollie catchment approximately 20 km east of the main divide of the central Southern Alps, New Zealand. The main objective is to apply a frequently used assimilation method, the ensemble Kalman square root filter, to assimilate remotely sensed snow covered area into the model and evaluate the impacts of this approach on simulations of snow water equivalent.

A 250 m resolution remotely sensed data from Moderate Resolution Imaging Spectroradiometer (MODIS), specifically tuned to the study location was used. Temperature and precipitation were given on a 0.05° latitude/longitude grid. Precipitation was perturbed as input into the model, generating 100 ensemble members, which represented model error. Only observations of snow covered area that had less that 25 % cloud cover classification were used in the assimilation precess. The error in the snow covered area observations was assumed to be 0.1 and grow linearly with cloud cover fraction up to 1 for a totally cloud covered pixel. As the model was not calibrated, two withholding experiments were conducted, in which observations withheld from the assimilation process were compared to the results. Two model states were updated in the assimilation, the total snow accumulation state variable and the total snow melt state variable. The results of this study indicate that the model underestimates snow storage at the end of winter and/or does not detect snow fall events during the ablation period. The assimilation method only affected simulated snow covered area and snow storage during the ablation period. That corresponded to higher correlation between modelled snow cover area and the updated state variables. Withholding experiments show good agreement between observations and simulated snow covered area. This study successfully applied the ensemble Kalman square root filter and showed its applicability for New Zealand conditions.

1 Introduction

Accurate estimate of water content in seasonal snow cover is an important factor in runoff and flood forecasting (e.g. Elder et al. 1998, Turcotte et al. 2007), particularly in mid-latitude regions where snowmelt contribution is often the main component in spring runoff (Erxleben et al. 2002). As snow properties, such as snow cover and snow storage, often exhibit considerable temporal and spatial variability, large scale measurements are often heavily dependent on remote sensing (Andreadis & Lettenmaier 2006). In this study, a model will be used to predict seasonal snow storage in the Jollie Catchment, Southern-Alps New Zealand, and the effects of assimilation of remotely sensed snow covered area information will be evaluated using data withholding experiments.

In New Zealand the seasonal snow cover often exhibits high variability as precipitation can occur as rain at elevations up to 2500 m in mid winter and snow can fall in summer down to 500 m (Fitzharris et al. 1999). It has also been estimated by Fitzharris et al. (1999) that one-third of the New Zealand average annual runoff occurs during spring and that 40 % of the fluctuations in spring runoff can be explained by variations in snow melt and of 60 % by precipitation. Fitzharris & Grimmond (1982) demonstrated that seasonal snow storage is 33 % of annual runoff for the Fraser Catchment, which probably represents the upper limit of seasonal snow storage contribution for New Zealand, and long-term estimates indicate 15 % contribution of seasonal snow storage to annual inflow into hydroelectric storage lakes (Fitzharris 1987, Fitzharris & Garr 1995). In contrast with the relative importance of seasonal snow in New Zealand, very few systematic observations on snow depth and snow water equivalent have been conducted. Therefore, snow research in New Zealand has been described as a relatively young field of investigation (Fitzharris et al. 1999).

In order to describe the evolution of snow cover from autumn through spring melt, three fundamental factors are required (Liston 1999): 1) the end of winter (pre-melt) snow water equivalent distribution, 2) the melt rate, and 3) the depletion of snow covered area. These factors are also well known to be inter-related (Liston 1999). As the snow melts during spring, the surface under the snow cover is exposed, which in turn influences the melt rate and the surface energy fluxes.

The pre-melt snow water equivalent distribution affects the pattern of the snow covered fraction, as areas under thin snow cover are exposed earlier than areas covered with thick snow layer. Liston (1999) established the mathematical inter-relationships among these factors and demonstrated that knowledge of any two of them is sufficient to find an expression for the third one. Thus, given any usable snow melt model, this means that remotely sensed snow covered area information can be used to reconstruct the pre-melt snow water equivalent distribution.

A number of studies have shown that the resulting snow water equivalent distribution is strongly controlled by topography and weather patterns (e.g. Hartman et al. 1999, Anderton et al. 2004, Balk & Elder 2000). In New Zealand, the snow water equivalent distribution has been explained by the so-called snow wedge model (Fitzharris 1979, Fitzharris et al. 1999). Each storm leaves a wedge-like snow pattern with increasing snow depth from the snow line (i.e. freezing level of the storm) to higher elevations. Series of such snow storms during the winter time build up the resulting snow wedge pattern. Although this model suggests that snow water equivalent distribution depends strongly on elevation, it is also recognized (Fitzharris 1979) that local factors such as aspect, slope, and snow drift are very important for the resulting local snow water equivalent distribution.

As the factors influencing the local snow water equivalent distributions are generally similar from one year to the next, the patterns described by these distributions are expected to show little inter-annual variation at each location even though the snow storage can vary considerably (Liston 1999). The distribution of snow water equivalent is therefore assumed to be independent of the magnitude of snow storage.

In previous work the snow water equivalent distribution has been represented by a snow depletion curve (e.g. Luce et al. 1999, Luce & Tarboton 2004, Déry et al. 2005, Kolberg & Gottschalk 2006, Andreadis & Lettenmaier 2006) or the distribution has been assumed to be two-parameter lognormal (e.g. Liston 2004, Clark et al. 2006, Udnæs et al. 2007), two-parameter gamma (Skaugen et al. 2003) or other distributions, such as three-parameter lognormal, three-parameter beta and 3- to 5-parameter weighted combinations of normal and/or lognormal distributions (Kolberg et al. 2006). In this study, a two parameter lognormal distribution will be assumed where the parameters are related to the average snow water

equivalent and the coefficient of variation.

Remotely sensed snow covered area information has been used successfully in snow melt and runoff models (e.g. Yang et al. 2003, Clark et al. 2006, Dressler et al. 2006, Kolberg & Gottschalk 2006, Kolberg et al. 2006, Andreadis & Lettenmaier 2006, Ghanbarpour et al. 2007, Udnæs et al. 2007). Remotely sensed snow water equivalent has also been used (e.g. Derksen et al. 2003, Andreadis & Lettenmaier 2006, Pulliainen 2006, Dong et al. 2007), although generally lacking accuracy required by hydrologic models (e.g. Hall & Riggs 2007, Dong et al. 2007). In this study, MODIS snow covered fraction maps with 250 m resolution are utilized. They are derived from multispectral fusion between MODIS 250 m bands and MODIS 500 m bands (Sirguey et al. 2008).

Remotely sensed snow covered area information has been used both as a direct input into a hydrological model (e.g. Tekeli et al. 2005, Yang et al. 2003, Luce et al. 1999, Schaper et al. 1999) or it has been used through various assimilation methods, including rule based updating (e.g. Udnæs et al. 2007, Dressler et al. 2006, McGuire et al. 2006), Kalman filtering (e.g. Kumar et al. 2008, Clark et al. 2006, Andreadis & Lettenmaier 2006), Bayesian filtering (e.g. Kolberg & Gottschalk 2006, Kolberg et al. 2006) and particle filtering (e.g. Moradkhani et al. 2005*a*). The assimilation methods, other than rule based updating, are statistical methods that use the covariance between the assimilated observable and modelled states to update the latter. Reliable estimates of the uncertainty in both remotely sensed data and model states are critical for these assimilation filters (Dong et al. 2007).

This study follows a framework presented by Clark et al. (2006), utilizing the ensemble square root Kalman filter to assimilate remotely sensed snow covered area information into the model used.

1.1 Main objectives and data sources

The main objectives of this study are to:

1. use a snow model to predict snow water equivalent in the Jollie Catchment, east of Aoraki/Mt Cook National Park,

2. assimilate snow covered area information into the model, and

3. evaluate the impacts of assimilation on snow water equivalent.

The snow model component of TopNet (Clark et al. 2008), which is a distributied hydrological model that has been developed by NIWA (Natural Institute of Water and Atmospheric Research, New Zealand), will be used and all forcing data will also be provided by NIWA.

Ensemble square root Kalman filter will be used to assimilate remotely sensed snow covered area information into the model. The remotely sensed data is provided by GLIMS NZ, School of Surveying at the University of Otago, and delivered as the snow fraction at 250 m resolution.

1.2 Thesis layout

The thesis consists of seven chapters including the introduction, Chapter 1. The study site will be described in Chapter 2 followed by a discussion about the data and the model in Chapters 3 and 4 respectively. In Chapter 5 the assimilation method used in this study will be described and an evaluation of its performance will be given in Chapter 6. Finally, Chapter 7 highlights the main conclusions.

2 Study site

The site chosen for this study is the Jollie Catchment. This catchment is situated on the South Island of New Zealand in the Canterbury region, Mackenzie district. It is close to the centre of the Southern Alps mountain range and on the east side of the main divide. The Jollie Catchment is a narrow valley defined by mountain ranges on both sides with steep slopes (see Figure 2.1). Alpine zones cover more than 50 % of the catchment and combined with tussock zones the coverage is just under 90 % (see Figure 2.2). The Jollie Catchment is just under 25 km long and is oriented North-north-east to South-south-west with mean elevation close to 1180 m a.s.l., ranging from 590 m a.s.l. near the outlet up to 2740 m a.s.l. on the highest mountain peak. The catchment is relatively small, around 140 km^2, and delivers water through the Jollie River via the Tasman river into Lake Pukaki, which contains half of the total controlled hydroelectric water storage on the South Island (Fitzharris 1992). The Jollie Catchment is therefore a small part ($\sim$ 10 %) of a larger Pukaki basin.

The climate near the study site region is very much affected by terrain at local scales and by the circumpolar westerly windbelt at synoptic scales (e.g. Sturman et al. 1999). While regions to the west of the main divide of the Southern Alps are characterized by above-average precipitation compared to nearby climate regions, areas on the east side are drier. Temperature comparison does not show as distinct results, according to empirical estimates by Norton (1985). Comparison of temperature at 1000 m a.s.l. in the Jollie and Paringa, which is at same latitude to the west of the main divide, show slightly colder temperatures in the Jollie, i.e. 11.8 °C versus 11.2 °C average temperatures in January and 1.0 °C versus 1.8 °C in July for the Jollie and Paringa respectively (Norton 1985).

As the Southern Alps reach over 3000 m a.s.l. west of the study site, and generally exceed 2000 m a.s.l. at other locations, they provide excellent conditions for orographic uplift. This results in increased precipitation, often as much as three to four times sealevel values near or west to the main divide (Fitzharris 1992). On the east side however, much less precipitation is experienced due to rain-shadow effects (Sturman et al. 1999) even though a spillover precipitation from the west is the main component of water on the east side (Fitzharris 1992). An estimated

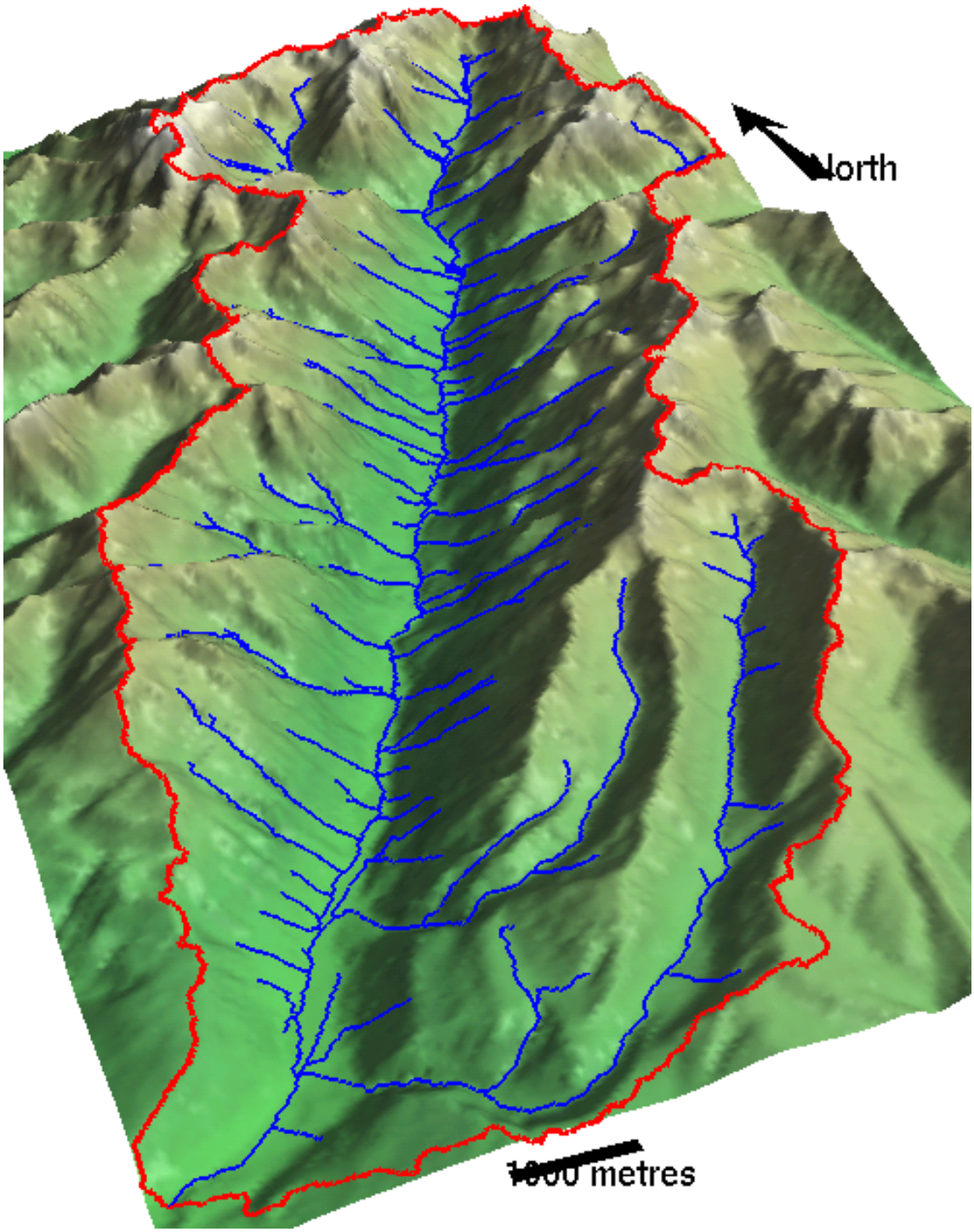

Figure 2.1: The Jollie Catchment outlines and the river network (Snelder & Biggs 2002) depicted on a digital elevation model (Barringer et al. 2002).

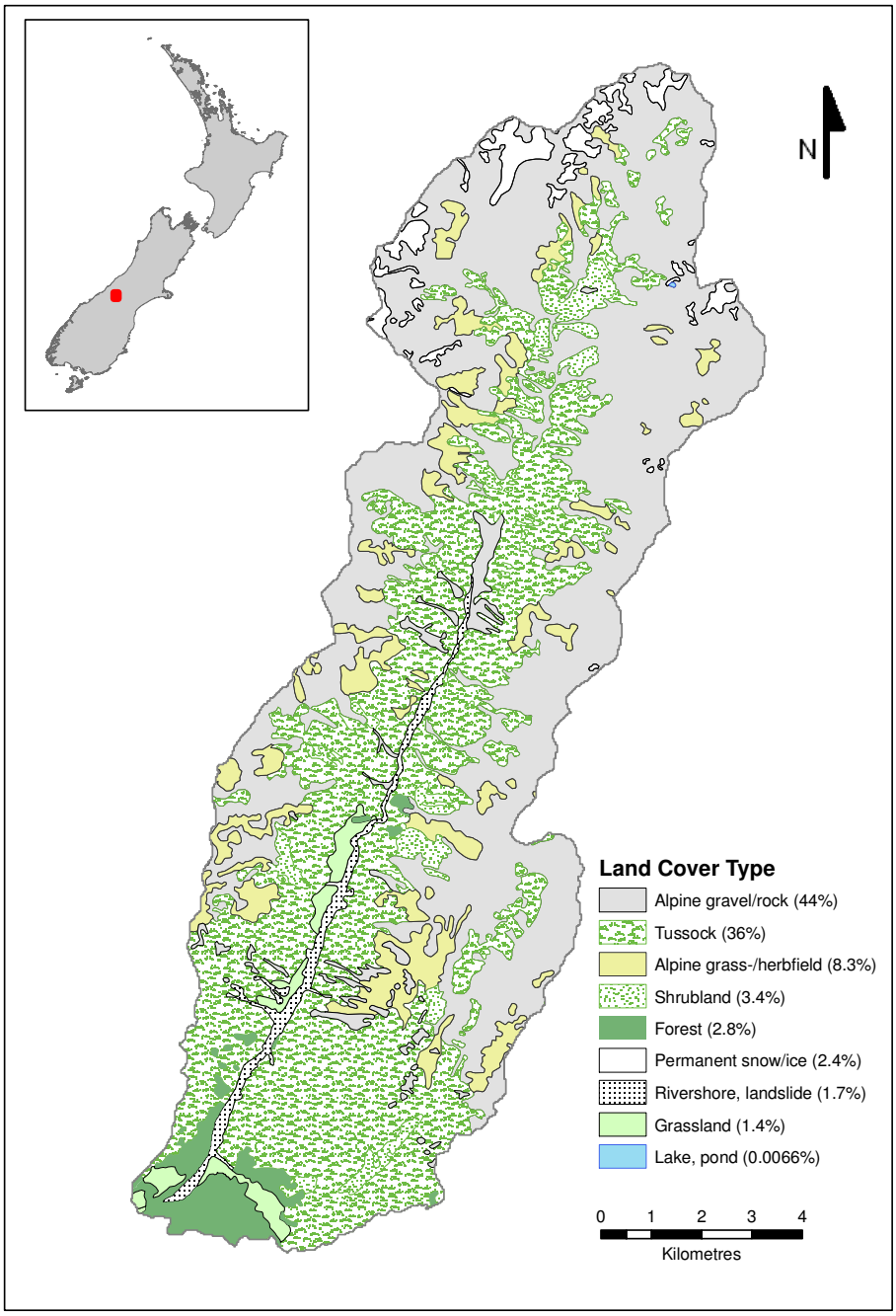

Figure 2.2: Land cover types in the Jollie Catchment. Land cover information after Terralink International Limited (2004).

trans-alpine precipitation profiles in Henderson & Thompson (1999), show that annual precipitation to the west of the divide exceed 10,000 mm while annual precipitation in the Jollie is only about 3000 mm.

During the cool seasons, most precipitation can be expected to fall as snow above 1000 m a.s.l. but as rain at lower elevations. The seasonal snowline in winter is highly variable but lies on average between 1000 m a.s.l. to 1300 m a.s.l., ascending to above 2000 m a.s.l. at the end of summer (Fitzharris 1992).

3 Data

All data used in ths study, comprising forcing data (i.e. input data), snow covered area data, and ancillary data, will be described below. They are all used for the period from 1 February 2006 to 31 January 2007.

3.1 Forcing data

Data used to force the snow model (i.e. input data) are minimum and maximum temperature and accumulated precipitation (see Figures 1(a) and 1(b) below). These data are measured for every 24 hour period from 9 am to 9 am New Zealand local time. These datasets were both supplied by NIWA (National Institute of Water and Atmospheric Research) and are based on their network of climate stations throughout New Zealand. The datasets are given on a 0.05° latitude/longitude grid (i.e. 4.2 km North-South versus 5.5 km East-West grid size) covering all of New Zealand. The grid values are interpolated from observations at over 500 climate stations by applying a *trivariate second-order derivative thin plate smoothing spline* (Tait et al. 2006, Tait & Zheng 2007).

As the majority (i.e. 93 %) of the climate stations are below 500 m a.s.l. it can be problematic to estimate climate variables accurately in higher elevation regions that are generally outside the climate station network (Tait et al. 2006). Therefore, for such regions, additional uncertainty in climate variable estimates is inevitable and depends, to some extent, on the interpolation algorithm used and its implementation.

The *thin plate smoothing spline* interpolation method has been shown to perform well for New Zealand conditions (e.g. Tait et al. 2006, and citations therein). This algorithm fits a three dimensional surface to observations, allowing for some errors so the surface does not need to fit the observations exactly, which gives a smoother surface (e.g. Tait et al. 2006). The surface roughness is also controlled through the *order of derivative* parameter and the method is often implemented as either *bivariate* (i.e. with latitude and longitude as the independent parameters) or *trivariate* (i.e. with latitude, longitude and additional surface variable as the independent parameters). The optimal surface is found through a process called

minimizing the generalized cross validation (GCV). In this process, one datapoint is withheld from all the other datapoints and not used used when the surface is fitted. The error of the withheld datapoint is then found. This process is repeated for all the datapoints and the surface that minimizes the mean error is the desired optimal surface (Tait et al. 2006).

This interpolation method was applied to the maximum and minimum temperature datasets with elevation as the third independent parameter along with latitude and longitude (Tait & Zheng 2007) and to the precipitation dataset with a *mean annual precipitation surface from the period 1951 to 1980* as the third independent parameter (Tait et al. 2006). This precipitation surface was obtained from a hand-drawn contour map of the mean annual precipitation based on observation at climate stations from the period 1951 to 1980 (New Zealand Meteorological Service 1985). For regions with few or no observations, which included most of the mountainous areas, an *expert* interpolation by visual observation of rainfall was applied (Tait et al. 2006). This contour map showed overall more realistic rainfall in the mountainous areas compared to using elevation as the third independent variable in the spline method. This comparison was based on short term measurement, observed river flows and some high-resolution model runs (Tait et al. 2006). Consequently, when this mean annual precipitation surface was used as the independent variable in the spline method instead of elevation, the error was reduced when compared to average annual runoff. Although this precipitation surface gives a better result, a *constant spatial precipitation pattern* is an underlying assumption, which is evidently not correct when considering for example a winter-time southerly frontal storm and a summer-time convective system (Tait et al. 2006). This is however, considering the spatial distribution of existing climate stations, the best available estimate of the precipitation. Close inspection of Figure $6(b)$ in Tait et al. (2006, p. 2108) indicates that the estiated precipitation, given by the method just described above, is likely to underestimate actual precipitation by 10 % to 25 % in the Jollie Catchment.

As the model time step is one hour, both the temperature and the precipitation need to be disaggregated from daily values to hourly. Hourly values of temperature are disaggregated by fitting a sine curve to the maximum and minimum daily

temperature. This can be expressed as

$$T(H) = \frac{1}{2}\sin\Big(\frac{2\pi}{24}(H+\varphi)\Big)(T_{max}-T_{min}) + \frac{1}{2}(T_{max}+T_{min}) \tag{3.1}$$

where T_{max} and T_{min} are maximum and minimum daily temperature respectively, H is the hour of the day and φ is a parameter that controls the time of the minimum and maximum temperature.

The precipitation is disaggregated by applying a discrete multiplicative random cascade model (Rupp et al. 2006). This model has the desirable property that it can resemble the intermittent pattern often seen in a real rainfall. In this model, the daily precipitation interval (i.e. 24 hours) is divided into smaller timesteps by multiplying it with a random weight, a process repeated over many cascade levels until a required temporal resolution is obtained (i.e. 1 hour) (Rupp et al. 2006).

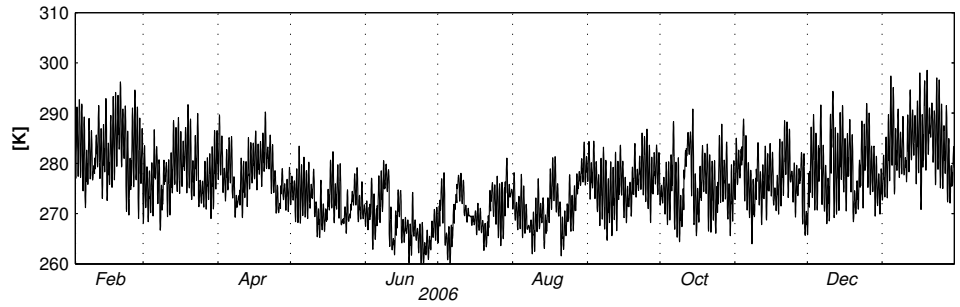

(a) Air temperature.

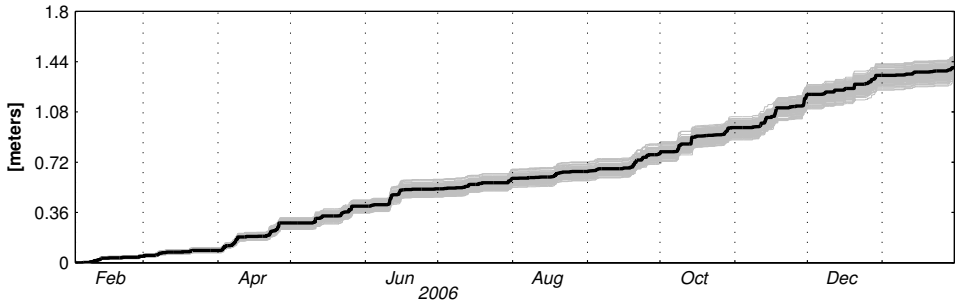

(b) Accumulated precipitation. The thick line is the control run and the grey lines are other ensemble members (see section 4.1 for ensemble generation).

Figure 3.1: Forcing data for the highest sub-basin in the Jollie Catchment (see also Figure 3.2, p. 13).

3.2 Snow covered area

The fractional snow covered area dataset used in this study is derived from the Moderate Resolution Imaging Spectroradiometer (MODIS) available on two satellites, Terra and Aqua. The Terra satellite was launched in December 1999 and Aqua in May 2002 (e.g. Salomonson & Appel 2004) and their primary purpose was to enable regional to global study of both the atmosphere and the Earth's surface on daily basis (Hall et al. 1995). Although MODIS offers fractional snow maps at 500 m resolution as a standard product (e.g. Hall & Riggs 2007), they are not utilized in this study. Instead, a 250 m resolution fractional snow maps tuned specifically to the study region, were used. These maps were produced by Pascal J. Sirguey at the University of Otago, New Zealand, and cover an area of $18,000\,\mathrm{km}^2$, including the study site (see Figure 3.2).

The data used to produce the fractional snow maps were MODIS-Terra Level 1B swath data products: geolocations at 1 km resolution (MOD03) and calibrated radiances at resolution 1 km (MOD021KM), 500 m (MOD02HKM), and 250 m (MOD02QKM) (Sirguey 2008). Two 250 m resolution spectral bands and five 500 m resolution spectral bands were used for the snow cover detection (see Table 3.1). The normalized difference snow index (NDSI) is often used to discriminate snow by taking advantage of the contrast between the reflectance of snow in the visible region (high reflectance) and the infrared region (low reflectance) of the spectrum. MODIS algorithms use bands $b4$ and $b6$, representing high and low reflectance of snow respectively, e.g.

$$NDSI = \frac{b4 - b6}{b4 + b6} \tag{3.2}$$

after Salomonson & Appel (2004), to calculate the snow index which only gives the snow cover maps at 500 m resolution.

To improve the resolution to 250 m, Sirguey et al. (2008) used wavelet-based multiresolution analysis to fuse high spatial content of bands $b1$ into bands $b3$ and $b4$ and high spatial content of band $b2$ into bands $b5$, $b6$, and $b7$ (see Table 3.1).

With bands $b3$ to $b7$ transformed to 250 m resolution, a snow fractional maps were produced in a postprocessing procedure, which involved topographic and atmospheric correction as well as spectral unmixing technique (Sirguey et al. 2008). Topographic correction was achieved by adapting a model developed by Richter

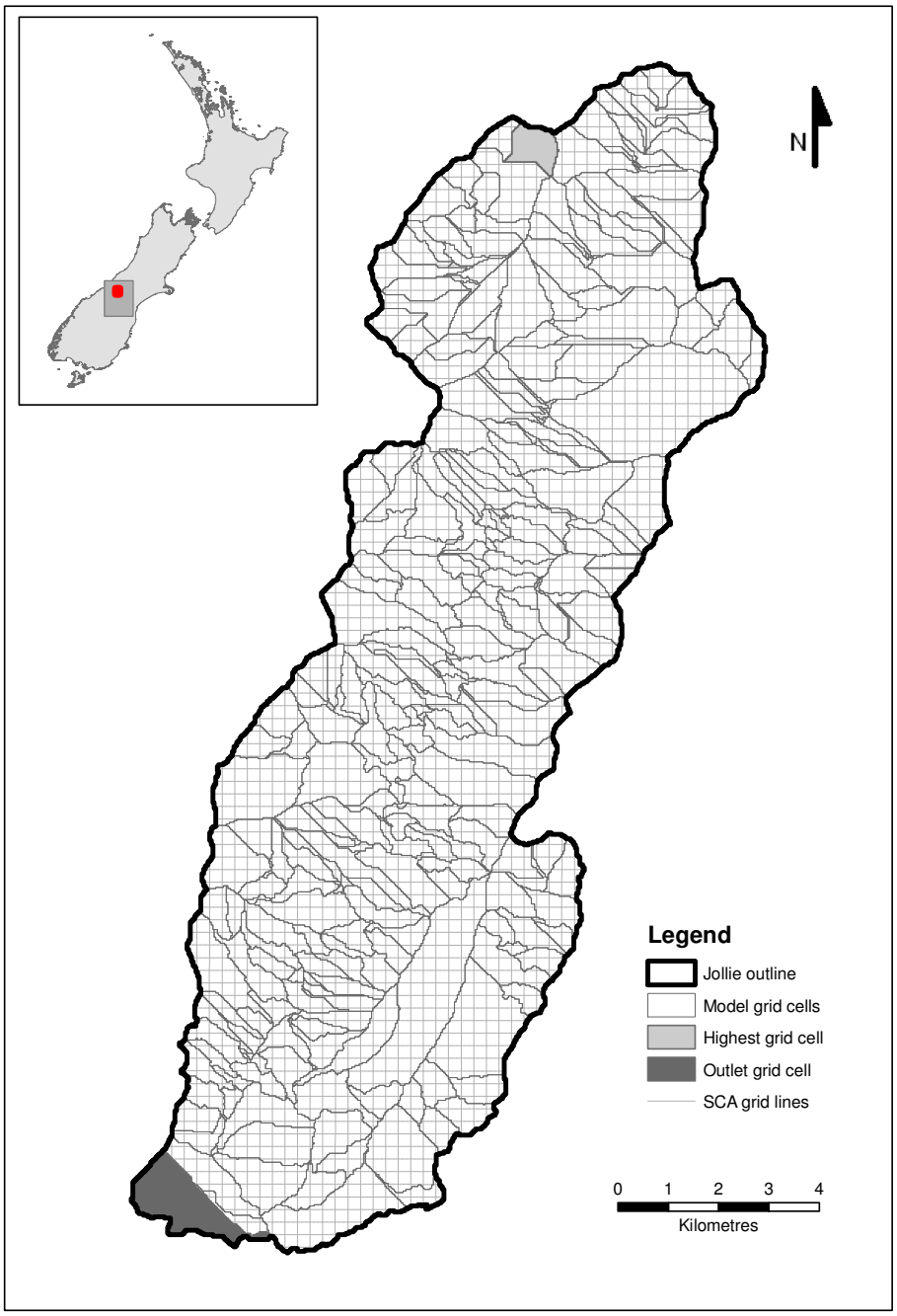

Figure 3.2: Model and data grid cells in the Jollie catchment. Delineation of sub-basins is described in Snelder & Biggs (2002). The gray rectangle on the inset map represents the area covered by the snow fraction maps.

Table 3.1: MODIS bands used for snow detection.

Band number	Spectral band [nm]	Resolution [m]
$b1$	620–670	250
$b2$	841–876	250
$b3$	459–479	500
$b4$	545–565	500
$b5$	1230–1250	500
$b6$	1628–1672	500
$b7$	2105–2155	500

(1998). This correction accounts for effects such as elevation, shadows, terrain-reflected radiation, and illumination angles, which all can contribute considerably to misinterpretation of the data in a rugged and snowy environment. Clouds can also be a significant source of errors in the data, as misclassification is frequent between snow and clouds (e.g. Hall et al. 1995). A MODIS *water vapour product* algorithm was used for cloud detection along with reflective and emissive bands at 1 km resolution. This algorithm was adopted by adjustng thresholds and tests to minimize snow/cloud misclassification in the region. An adequate atmospheric correction model is necessary to account for processes such as absorption (e.g. by ozone), emmision (i.e. by atmospheric constituents) and scattering (e.g. by aerosols) in the atmosphere. These processes modify the detected remotely sensed signal and must be accounted for to reduce the errors in the data. An atmospheric correction model developed by Bird & Riordan (1986) was applied and necessary estimates of ozone were taken from the *Total Ozone Mapping Spectrometer* zonal monthly average and aerosol optical depth was estimated through visibility measurements at Mount Cook airport (Sirguey et al. 2008).

After the topographic and atmospheric corrections, a spectral unmixing technique was applied to estimate the fractional snow covered area within each pixel (Sirguey et al. 2008). A constrained linear unmixing method was adopted from Keshava (2003) and used eight endmembers with known spectral signatures, obtained from measurements in the field or from corrected MODIS images (Table 3.2) The application of this technique then gives estimates of the proportion of each

Table 3.2: Selected endmembers for the constrained spectral unmixing technique.

	Endmember
1	Ice
2	Rock, bright
3	Rock, dark
4	Snow, class 1
5	Snow, class 2
6	Snow, class 3
7	Vegetation, bright
8	Vegetation, dark

endmember in a pixel by decomposing the collection of observed spectra within the pixel (Keshava 2003).

Validation of these fractional snow maps has been done by comparing them with snow maps derived from ASTER 15 m resolution data. This comparison showed good results with the mean absolute error less than 0.1 (Sirguey et al. 2008). For comparison, the mean absolute error of fractional snow cover within the MODIS 500 m resolution pixel is estimated to be less than 0.1 for the entire range of snow fraction from 0.1–1.0 (Salomonson & Appel 2004). The errors are therefore similar in these two snow maps, but the higher resolution of the snow maps used in this study is a great advantage. It has, however, been acknowledged that the accuracy of any snow map is difficult to estimate by inter-comparison because it is not know which snow map is the *truth* or closest to the *truth* (Hall et al. 2002).

For this study, the error associated with the fractional snow covered area information is estimated to be 0.1 for a cloud free pixel and increase linearly with increasing cloud cover up to 1.0 for totally cloud covered pixel as for such pixels, the information about snow cover is not known.

As the fractional snow cover is given for each pixel at resolution 250 m, it needs to be aggregated onto the larger model grid cells (see Figure 3.2, p. 13). It is done by taking a weighted sum of all pixels within each model grid cell, where the weight of each pixel is equal to the fractional area it occupies within a model grid cell.

3.3 Ancillary data

A different source of data that describes the topology of the Jollie catchment and other necessary attributes are also required by the model (see Table 3.3). These data are mostly derived form the River Environment Classification database (REC) (Snelder & Biggs 2002), which stores spatial pattern information in river ecosystems by applying a controlling factor approach based on fluvial processes (Snelder & Biggs 2002). The REC database derives the watersheds and river network informatin from a three dimensional digital elevation map (DEM) (Barringer et al. 2002) with minimum area threshold of $0.02\,\mathrm{km}^2$, which garantees congruence with the $1:50,000$ topographic map of New Zealand.

The sub-basins (i.e. the model grid cells) derived from the REC database can be seen seen on Figure 3.2 (p. 13), which covers the Jollie catchment. The catchment is split up into 297 sub-basins, with mean area of about $0.5\,\mathrm{km}^2$. The highest subbasin is $0.7\,\mathrm{km}^2$ with mean elevation 2038 m a.s.l. while the outlet subbasin is $2.0\,\mathrm{km}^2$ with mean elevation 588 m a.s.l..

Table 3.3: Spatial parameters derived from ancillary data.

Parameter	Unit	Description	Data source
Atmospheric lapse rate	$\mathrm{K/m}$	Assumed uniform with value $0.0065\,\mathrm{K/m}$	—
Elevation	m a.s.l.	Mean elevation for each sub-basin	REC
Area	m^2	Area occupied by each sub-basin	REC
Location	lat/lon	Location of the centre of each sub-basin	REC

4 Model

The model used in this study is *TopNet* (Clark et al. 2008, Bandaragoda et al. 2004), a model that is being developed by NIWA (National Institute of Water and Atmospheric Research) and is currently used as the hydrological component of a nationwide flood forecasting system for New Zealand (Clark et al. 2007). This is a distributed hydrological model and contains two fundamental components: a water balance model and a network routing model (Clark et al. 2008). The water balance model simulates water fluxes and storages for each *sub-basin* (i.e. each model grid cell) within the model boundary. Water storages are divided into five components: canopy storage, snowpack storage, soil (i.e. root zone) storage, aquifer storage and overland flow storage. The network routing model uses one dimensional Lagrangian kinematic wave routing scheme to transmit runoff from each sub-basin into and through the river network. In this scheme the runoff is propagated through the river network as *particles* that eventually leave the model boundary through the outlet sub-basin (Clark et al. 2008).

In this study, only the snow storage component of the *TopNet* model will be used, configured as a temperature index snow model. It is run on hourly timesteps and requires precipitation and temperature as forcing data (i.e. input data) (see Chapter 3.1). In the following sections the data selection and ensemble generation will be briefly described followed by an overview of the snow model.

4.1 Data selection and ensemble generation

As described earlier (Chapter 3.1, p. 9) the input data is given on a 0.05° latitude/longitude grid. A point on this grid that is closest to the centre of a given sub-basin is selected as an input data point for that sub-basin. The selected input data values from the precipitation grid are used unchanged while the temperature values are corrected because of general difference in elevation between the centre of the sub-basins and the selected grid points. In this correction, a constant lapse rate ($0.0065\,\mathrm{K/m}$ see Table 3.3, p. 16) is assumed.

When an ensemble of model trajectories is needed the precipitation is perturbed for all except the first ensemble member, which serves as a control en-

semble member. As discussed in more detail in Chapter 5, this gives an estimate of the model output error that is necessary in the assimilation process. The precipitation perturbation is achieved by applying a geostatistical method (Clark & Slater 2006), which involves creating a spatially correlated random field at the data grid points. This method preserves the space-time correlation within the original dataset (Clark et al. 2006) and is applied *before* the dataset is disaggregated to hourly time steps.

4.2 Snow model

The framework for the snow model can be described by a state equation for snow water equivalent (SWE $[\mathrm{kg/m^2}]$) as

$$\frac{dSWE}{dt} = a_s - m_s - s_s, \tag{4.1a}$$

$$a_s = \begin{cases} 0, & \text{if} \quad T \geq T_{accm}, \\ p, & \text{if} \quad T < T_{accm}, \end{cases} \tag{4.1b}$$

$$m_s = \begin{cases} M_f(T - T_{melt}), & \text{if} \quad T \geq T_{melt}, \\ 0, & \text{if} \quad T < T_{melt} \quad \text{or} \quad SWE = 0, \end{cases} \tag{4.1c}$$

$$s_s = 0, \tag{4.1d}$$

where a_s is the rate of accumulation ($[\mathrm{kg/m^2s}]$), m_s is the snow melt rate ($[\mathrm{kg/m^2s}]$), s_s is the rate of sublimation ($[\mathrm{kg/m^2s}]$), p is the precipitation rate ($[\mathrm{kg/m^2s}]$), T is air temperature ([K]), T_{accm} is the temperature threshold to distinguish between rain and snow ([K]), M_f is the melt factor ($[\mathrm{kg/m^2sK}]$) and T_{melt} is the temperature threshold for snow melt ([K]). Sublimation is included for completeness above but is not simulated in the configuration of the model used in this study, and is thus set to zero in (4.1d) above. Both the precipitation, p, and temperature, T, enter (4.1) as input data and M_f, T_{accm} and T_{melt} are model parameters.

While (4.1) is in itself a complete snow model, three main enhancements are introduced below involving precipitation under-catch, prescribed log-normal distribution of SWE and dependence of the melt factor on season, snow albedo, and rain on snow events.

Table 4.1: Snow model parameters.

Parameter	Value	Unit	Description
T_{accm}	274.16	K	Temperature threshold for snow accumulation
T_{melt}	274.16	K	Temperature threshold for snow melt
CV	1.0	–	Coefficient of variation in the distribution of *snow water equivalent* (SWE)
ϕ	1.0	–	Correction for under-catch of precipitation (correction turned off)
r	864,000	s	Time scale for the reduction in snow albedo (10 days)
$\overline{M}_f$	$2/86,400$	$\mathrm{kg/m^2\,s\,K}$	Mean melt factor
M_f^{seas}	$2/86,400$	$\mathrm{kg/m^2\,s\,K}$	Seasonal amplitude of the melt factor
M_f^a	$3/86,400$	$\mathrm{kg/m^2\,s\,K}$	Reduction in melt factor immediately after fresh snowfall
M_f^{ros}	$2/86,400$	$\mathrm{kg/m^2\,s\,K}$	Addition to melt factor for rain-on-snow events

Underestimation in precipitation measurements due to wind undercatch during snow events can often hinder snow model performance (e.g. Fassnacht 2007). The true (i.e. unbiased) precipitation, A, is therefore obtained by adding the estimated undercatch to the measured precipitation. This can be done by by multiplying the precipitation with a dimensionless correction parameter, ϕ, according to

$$A = \begin{cases} 0, & \text{if} \quad T \geq T_{accm}, \\ p\phi, & \text{if} \quad T < T_{accm}. \end{cases} \tag{4.2}$$

As can be seen in Table 4.1 this correction parameter is set to one in this study, thus disabling the bias correction.

The estimation of the melt factor M_f in (4.1c) can be improved by accounting for temporal changes in melt energy that are not related to the temperature. This can be expressed by

$$M_f = \max\left(\overline{M}_f + \delta M_f^{seas} + \delta M_f^a + \delta M_f^{ros}, 0\right), \tag{4.3a}$$

where $\overline{M}_f$ is the mean melt factor, δM_f^{seas} is the change in the melt factor associated with seasonal variability in melt enrgy, δM_f^a is the reduction in melt energy due to higher snow albedo immediately after snowfall, and δM_f^{ros} is the additional melt energy available during rain on snow events. The max function is necessary to ensure non-negative melt factor.

The seasonal variability can be parameterized as a sine curve

$$S_i = \begin{cases} -\sin\left(\dfrac{d2\pi}{366} + 0.551\pi\right), & \text{for the northern hemisphere (i.e. latitude} > 0), \\ \sin\left(\dfrac{d2\pi}{366} + 0.551\pi\right), & \text{for the southern hemisphere (i.e. latitude} < 0), \end{cases} \tag{4.3b}$$

where S_i is the solar index, d is the number of days since 1 January of the current year, and the phase shift, 0.551π, is used to adjust the sine curve to the seasons so the melt factor is lowest in the southern hemisphere on 21 June and on 21 December in the northern hemisphere. This sine curve parameterization, expressed with the solar index S_i, can now be used to compute the seasonal changes in melt energy, δM_f^{seas}, according to

$$\delta M_f^{seas} = M_f^{seas} S_i, \tag{4.3c}$$

where M_f^{seas} is the seasonal amplitude of the melt factor (see Table 4.1).

As new fallen snow has higher albedo than older snow (e.g. Flanner & Zender 2006), the amount of melt energy available is reduced immediately after snowfall event. This can be parameterized as

$$\delta M_f^a = -M_f^a \exp\left(-\frac{d_{snow}}{r}\right), \tag{4.3d}$$

were d_{snow} ([s]) is the time since fresh snowfall, r ([s]) is the timescale for the decrease in snow albedo, and M_f^a is the reduction in melt factor associated with the shift in snow albedo immediately after snowfall.

An increase in the melt factor due to a rain on snow event can be parameterized

in a simple way by

$$\delta M_f^{ros} = \begin{cases} 0, & \text{if} \quad p\phi - a_s = 0, \\ M_f^{ros}, & \text{if} \quad p\phi - a_s > 0, \end{cases} \tag{4.3e}$$

where M_f^{ros} is the additional melt energy during rain on snow events, $p\phi$ is the unbiased precipitation (see Equation (4.2)), and a_s is the rate of snow accumulation (see Equation (4.1b)).

The snow water equivalent distribution can have important effects on the snowmelt, as areas under thin snow are exposed earlier than areas with a thick snow layer that can contribute melt late into the summer. In this model, the variability in snow water equivalent is prescribed by a two parameter log-normal distribution (Liston 2004) given by

$$f(D) = \frac{1}{D\zeta\sqrt{2\pi}} \exp\left(-\frac{1}{2}\left(\frac{\ln(D) - \lambda}{\zeta} \right)^2 \right), \tag{4.4a}$$

with

$$\lambda = \ln(\mu) - \frac{1}{2}\zeta^2, \tag{4.4b}$$

and

$$\zeta^2 = \ln\left(1 + CV^2\right). \tag{4.4c}$$

Here, D ($[\mathrm{kg/m^2}]$) is snow water equivalent, and the two distribution parameters, λ and ζ, in (4.4a) are related to the mean, μ, and the coefficient of variation, CV, according to (4.4b) and (4.4c). The coefficient of variation, CV which is equal to the ratio of the standard deviation to the mean, is given as a model parameter and assumed uniform over all the sub-basins (see Table 4.1).

When this distribution of snow water equivalent (SWE) is implemented it is convenient to assume that the distribution of SWE is entirely due to snow accumulation processes and that the melt is uniform over a sub-basin (Liston 2004). This is done by keeping track of two state variables: the total snow accumulation, μ which represents the mean in (4.4a) when no melt has occurred, and the total snow melt over a season, D_m (see Figure 4.1, p. 22; and Table 4.2, p. 23). The snow covered area (SCA) and snow water equivalent (SWE) can then be computed

by integrating over the probability distribution from D_m according to

$$SCA = \int_{D_m}^{\infty} f(D)\, dD, \tag{4.4d}$$

and

$$SWE = \int_{D_m}^{\infty} (D - D_m) f(D)\, dD. \tag{4.4e}$$

At the time when the accumulated snowmelt, D_m, results in total meltout (within some tolerance) both the total accumulation and melt state variables are reset to zero (e.g. March on Figure 4.1 for some ensemble members). In the next snowfall event, the total accumulation state variable starts increasing again, and will not be reset to zero unless total meltout occurs.

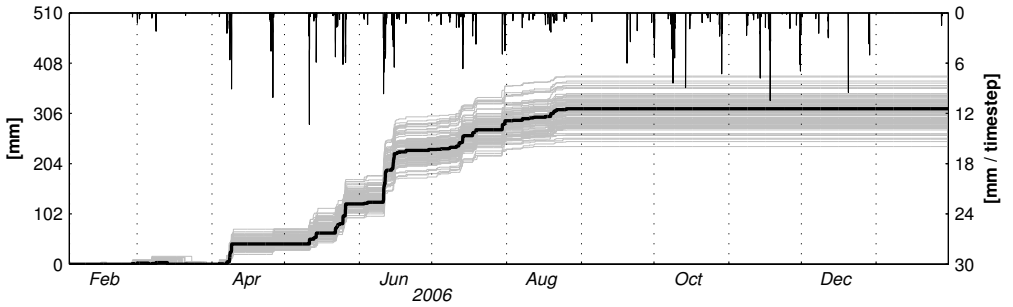

(a) Total snow accumulation state variable, μ, and snow accumulation per timestep for the control run (on the upper axis).

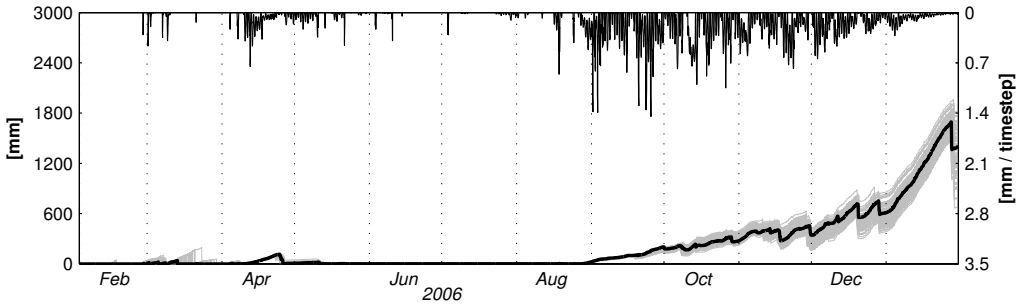

(b) Total snow melt state variable, D_m, and snow melt per timestep for the control run (on upper axis).

Figure 4.1: Total snow accumulation, μ, and melt, D_m, state variables for the highest sub-basin (see Figure 3.2, p. 13). The model ensemble, resulting from the perturbed precipitation input data, is shown as gray lines and the control run is shown as black thick line.

Table 4.2: Snow model states.

State	Unit	Description
SWE	$\mathrm{kg/m^2}$	Mean basin snow water equivalent
SCA	–	Fractional snow covered area
μ	$\mathrm{kg/m^2}$	Total mass in the accumulation array
D_m	$\mathrm{kg/m^2}$	Total mass in the melt array
d_{new}	s	Time since fresh snowfall

When new snowfall interrupts melt (i.e. snowfall occurs when the total snow melt state variable, D_m, is positive), as is not uncommon, the water content in the newfallen snow is used to decrease the total snow melt state variable, D_m, instead of adding it to the total snow accumulation state variable, μ. This can clearly be seen in Figure 4.1 above, where snowfall events cause the total snow melt state variable to shift to lower values. If more water content is in the newfallen snow than is present in the total melt state variable, the melt state variable is reduced to zero and the rest is added to the total accumulation state variable. This approach, to reduce the melt state variable, resembles the ablation period more realistically than adding all the snowfall to the total accumulation state variable (Liston 2004).

5 Assimilation

5.1 Background

Observations and models are integral parts of describing and researching natural phenomena. Observations give direct information about the state of some measurable quantities at certain points or subspaces in the universal four dimensional timespace. When these observations are stored and made available for potential users they become a valuable resource of information, which can be utilized in many different ways to gain a deeper understanding of the natural laws and processes involved.

For a given physical boundary within which some natural processes are being investigated, these observations can serve as a boundary conditions. By collecting all knowledge about relevant physical attributes of the substances within this boundary and the governing processes involved, a model can be constructed. This model can then be used to simulate processes and fluxes within and across this boundary, driven by the observed boundary conditions.

Within the model system, a terminology frequently adopted in hydrologic applications, is to distinguish input-, state-, and output-variables (McLaughlin 2002). Input variables is a term used for observations that are used to drive or force the system, state variables provide a full description of the system behaviour, and output variables are observable physical quantities and are functions of the state variables.

At least two different approaches are available for observations to be used in a model. Firstly, they can be used as input variables and therefore used to force the model, such as temperature and precipitation in land surface models. Secondly, the observations can be merged with the model in an updating scheme where the model states are updated based on the deviations of the model output variables from the observations (e.g. Reichle 2008). This latter approach, to merge the observations with the model output, is called data assimilation. An example of observations that have been successfully used in data assimilation into land surface models are various remotely sensed information, such as soil moisture or snow covered area (e.g. Udnæs et al. 2007, Kumar et al. 2008, Clark et al. 2006,

Kolberg & Gottschalk 2006, Moradkhani et al. 2005*a*, Dunne & Entekhabi 2005, Reichle et al. 2002).

The success of data assimilation is largely dependent on accurate estimates of all sources of errors involved (Reichle 2008, Liu & Gupta 2007). This is true, both for errors associated with the observations being assimilated as well as errors associated with the model.

The errors associated with the observations consist of instrument errors, representativeness errors, and transformation errors (Liu & Gupta 2007, Tsuyuki & Miyoshi 2007). The instrument errors are dependent on the instrumentation used while the representativeness errors stem from scaling issues, e.g. through a change of scale resulting from interpolation, extrapolation, aggregation or disaggregation (e.g. Blöschl 1999). The transformation errors are associated with the transformation between the observation space and the state space in the cases where the model states are not directly observable and only related to the observations in a functional form.

At least three main sources of model errors have been acknowledged in the literature (e.g. Turner et al. 2008, Liu & Gupta 2007, Vrugt et al. 2005): structural errors, parameter errors, and data errors. Structural errors result from errors in the conceptual structure of the model, including errors associated with the definition of the system boundary, errors resulting from the mathematical implementation of the conceptual model, and errors in the conceptual model due to missing components or inappropriate assumptions. Parameter errors result from errors in parameter values in the model. Parameters are necessary to use in equation-based models (Liu & Gupta 2007) and they often represent spatially and temporally heterogeneous properties of the real system and are often not easily measurable. Thus, parameters are often estimated through model calibration or by prior knowledge. Data errors include errors in the initial conditions of the model and errors in the forcing (i.e. input) data, which result from instrumentation and representativeness (i.e. scaling) errors.

These three model error components contribute to an uncertainty in the model states and outputs and are therefore important to take into account when uncertainty in the model states or outputs is estimated. However, little is known about model errors (Ehrendorfer 2007, Liu & Gupta 2007), particularity structural er-

rors, which often have far more impact on hydrologic model states and outputs than both parameter and data errors (e.g. Abramowitz et al. 2006). Accurate estimation of model uncertainty can therefore often be problematic, especially for hydrologic models, which have been described as still being far from perfect (Moradkhani et al. 2005*b*). It has also been pointed out by Liu & Gupta (2007) that structural and parameter errors are often simply ignored in hydrologic data assimilation schemes.

As the state variables described in the model equations are never perfectly known and usually vary at scales smaller than model grid sizes, it is natural to treat them as random (i.e. stochastic) variables (e.g. McLaughlin 2002). To show how that can be done, following the formalism of Lewis et al. (2006), the model is represented by a mapping $\mathbf{M}$: $\mathbb{R}^n \rightarrow \mathbb{R}^n$ describing the evolution of the model states in discrete time steps. If the vector $\mathbf{x}'_k \in \mathbb{R}^n$ represents the model states at time k and $\mathbf{m}_0 \in \mathbb{R}^n$ represents an initial condition, then the model is given by $\mathbf{x}'_k = \mathbf{M}(\mathbf{x}'_{k-1})$, for $k \geq 1$ with $\mathbf{x}'_0 = \mathbf{m}_0$. The purpose of this model is to imitate nature, in which the *true* state $\mathbf{x}_k \in \mathbb{R}^n$ evolves similarly according to

$$\mathbf{x}_k = \mathbf{M}(\mathbf{x}_{k-1}) + \mathbf{w}_k, \qquad \mathbf{x}_0 = \mathbf{m}_0 + \mathbf{e}_0, \tag{5.1}$$

which differs only from the model through the random vectors $\mathbf{w}_k, \mathbf{e}_0 \in \mathbb{R}^n$.

Equation (5.1) describes in general a non-linear stochastic dynamical system, where $\mathbf{M}(\cdot)$ is considered to be a non-linear mapping and $\mathbf{x}_k$ is the *true* random state vector with the randomness entering through the noise vectors $\mathbf{w}_k$ and $\mathbf{e}_0$. As the mapping $\mathbf{M}(\cdot)$ stands for the solution of all the equations used to describe certain natural processes within the boundary of the model, the noise vector $\mathbf{w}_k$ must include errors stemming from all the different sources of model errors discussed above.

Parallel to the model, an observation system exists that produces observations at time l, represented by the vector $\mathbf{z}_l \in \mathbb{R}^m$, which is related to the *true* state vector $\mathbf{x}_l \in \mathbb{R}^n$ through

$$\mathbf{z}_l = \mathbf{h}(\mathbf{x}_l) + \mathbf{v}_l. \tag{5.2}$$

Here, $\mathbf{h}$: $\mathbb{R}^m \rightarrow \mathbb{R}^n$ is in general a non-linear mapping and $\mathbf{v}_l \in \mathbb{R}^m$ is a random noise vector representing the uncertainty associated with all sources of observa-

tion errors discussed above. Thus, the observation vector $\mathbf{z}_l$ is a random vector where the randomness enters through the noise vector $\mathbf{v}_l$. As the components in the state vectors are not always directly observable, this mapping is necessary to allow for a direct comparison between model states and observations.

In the notation introduced above, an assimilation problem consists of finding an optimal estimate $\widehat{\mathbf{x}}_k$ of $\mathbf{x}_k$ at a time k, given a set of observations $\mathscr{F}_l = \{\mathbf{z}_i \mid 1 \leq i \leq l\}$ at a time l. In this formulation, time is considered to be a discrete variable and $\mathbf{x}_k \in \mathbb{R}^n$ and $\mathbf{z}_l \in \mathbb{R}^m$ are considered to be continuous space variables where n is the number of model states and m is the number of observed physical quantities.

Three basic estimation problems exist: smoothing when $k < l$, filtering if $k = l$, and prediction when $k > l$. Smoothing uses all observations for some time interval to find an optimal estimate $\widehat{\mathbf{x}}_k$ of a state $\mathbf{x}_k$ *within* this interval, while filtering only uses observations prior to and up to the time when the optimal estimate is found. Prediction only uses prior observations to find estimates of future states. The terms *off-line* and *on-line* assimilation are often used, reflecting this difference between smoothing (i.e. $k < l$), and filtering or prediction (i.e. $k \geq l$) respectively.

As the variables in equations (5.1) and (5.2) are random vectors, their full description is given by their associated probability distributions. The assimilation problem of finding an optimal estimate is therefore equivalent to updating the probability distribution of the state vector, given a new observation. This updating scheme can be achieved through the Bayesian probability theory, where the prior belief, $p(\mathbf{x}_k)$, and additional information given by a new observation, $p(\mathbf{z}_k \,|\, \mathbf{x}_k)$, are combined to give an updated probability distribution of the state vector, given the new observation, according to

$$p(\widehat{\mathbf{x}}_k) \equiv p(\mathbf{x}_k \,|\, \mathbf{z}_k) \propto p(\mathbf{x}_k) p(\mathbf{z}_k \,|\, \mathbf{x}_k). \tag{5.3}$$

A general framework for the temporal evolution of the probability distributions associated with the random variables in (5.1) is given by the so called Kolmogorov's equation (also called the Fokker-Planck equation, not stated here) and together with the Bayesian updating formula, constitute the basis of a general non-linear filtering for stochastic systems (Miller 2007, Evensen 1994). Kolmogorov's equation is usually difficult to integrate except for special cases (McLaughlin 2002),

and the assimilation methods used in practice today therefore rely on various approximations and a number of assumptions ideally based on physical insights (Reichle 2008). The scientific difficulty of data assimilation is therefore to find algorithms that balance the competing requirements of being sufficiently simplified to be computationally affordable, while retaining some of the essential characteristics of the original theory (Mathieu & O'Neill 2008).

The most commonly used data assimilation methods in hydrology today, are Kalman filtering, particle filtering, and variational data assimilation (Liu & Gupta 2007).

The Kalman filter (KF) is a closed form solution of Kolmogorov's equation, discussed above, in the case when all the random vectors in (5.1) and (5.2), have associated normal (i.e. Gaussian) probability distributions and the model equations are linear. In the Kalman framework the observation and state covariance matrices are used to find an optimal estimate (i.e. an update) of the model states. The updated states are, in a sense, computed as a weighted average of the observation and the model representation of the observation (i.e. model output) where the weights are adjusted through the requirements of minimum squared error and minimum variance in the optimal estimate. Thus for an accurate model, an observation will be given much less weight than for an inaccurate model using the same observation. Another feature, unique to Kalman filters, is the temporal evolution of the state covariance matrix, which makes it possible to account for temporal changes in the state covariance matrix as it evolves through the model equations. As hydrologic models are often highly non-linear the basic form of the Kalman filter is rarely used. Therefore, more practical Kalman filters have been derived, such as the extended Kalman filter, the ensemble Kalman filter, and square root Kalman filters.

The extended Kalman filter (EKF) uses the first order linear approximation of the model equations to apply the basic Kalman filter framework. The extended Kalman filter approach is known to be both computationally intensive and often lacks stability for highly non-linear models (e.g. Miller et al. 1994). As an alternative to the extended Kalman filter, Evensen (1994) introduced the ensemble Kalman filter (EnKF). The ensemble Kalman filter approach utilizes a Monte Carlo framework, which lowers the dimensionality of the problem and saves computa-

tional time as well as allowing full non-linearities of the model equations. Square root Kalman filters (SRF) express the model state and error covariance matrices as a product of square root matrices. The basic idea of square root filters is to provide a numerically stable implementation of the Kalman filter and enable a reduced rank factorization, which saves computational time.

Particle filtering (PF) is a sequential Monte Carlo procedure, based both on independent random samples, called particles, from the probability distributions of the state variables and a set of weights associated with each particle (e.g. Moradkhani et al. 2005*a*). In essence, this is equivalent to approximating the true continuous probability distribution with a discrete probability distribution where the mass of each member (i.e. each particle) of the sample space is adjusted through the weights. Instead of updating the model states in the presence of a new observation, as in Kalman filtering, the *weights* are updated in particle filtering according to a Bayesian updating scheme. This approach relaxes the restrictive requirement of the probability distributions to be Gaussian (i.e. normal) as in Kalman filtering, and also allows for their propagation through non-linear model equations (Liu & Gupta 2007). Particle filtering is therefore applicable to both linear and non-linear models with Gaussian or non-Gaussian probability distributions.

A common problem with particle filters is the so-called degeneracy problem, where the weights of the particles degenerate over time, resulting in only one particle having all the weight after a few time steps (e.g. Moradkhani et al. 2005*a*, Wikle & Berliner 2007). This weight degeneracy is associated with high dimensionality of either the model states or the observations (Wikle & Berliner 2007) and can been reduced by applying resampling methods (e.g. Moradkhani et al. 2005*a*). Although the particle filter has been suggested as an alternative to the least square formulation Kalman filters by Ehrendorfer (2007) for highly non-linear models, Wikle & Berliner (2007) conclude that the ensemble Kalman filter is *arguably* a more practical choice for high dimensionality data assimilation problems found in meteorology and oceanography. For hydrologic data assimilation applications, results from Moradkhani et al. (2005*a*) have demonstrated the usefulness of particle filters in estimating both model parameters and states in hydrologic models.

Variational data assimilation (VDA) methods are in principle based on the Bayesian probability theory and seek to find an optimal estimate that maximizes the updated probability distribution of the model states. Estimates obtained in this way are frequently called *maximum a posteriori* estimates or *conditional mode* estimates and can be obtained by minimizing a so-called cost function (or objective function) that is introduced for the sake of convenience (Tsuyuki & Miyoshi 2007). The cost function is minimized by applying iterative methods such as the quasi-Newton method or the conjugate gradient method (Tsuyuki & Miyoshi 2007), in which an initial guess is iteratively updated until a convergence condition is met. At each iteration, these methods need the gradient of the cost function, which can be efficiently calculated by applying the adjoint method. The adjoint method needs the adjoint of the model, of which construction can both be a time consuming and an error prone process (Tsuyuki & Miyoshi 2007) and is one of the major obstacles of implementing variational data assimilation (Ehrendorfer 2007). The adjoint method also assumes that the model equations are differentiable with respect to the model states, an assumption often violated in highly non-linear models. Variational data assimilation methods are nevertheless more computationally efficient for complex and high-dimensional processes, compared to other data assimilation methods such as Kalman filters and extended Kalman filters (Liu & Gupta 2007, Wikle & Berliner 2007).

Variational data assimilation methods include variants such as one dimensional (1D-Var), three-dimensional (3D-Var), or four-dimensional (4D-Var), depending on the spatial and temporal dimensions of the state variables (e.g. Reichle 2008, Liu & Gupta 2007). Different from the Kalman filtering and particle filtering, the 4D-Var variational data assimilation method operates over a given time interval (i.e. time window or assimilation window) which contains a number of observations that are assimilated simultaneously. The value of the initial state within the assimilation window is then updated by minimizing the cost function and consequently, the values of other states within this time interval can be obtained by integrating the model equations forward in time using the updated initial state. The 4D-Var method is therefore a *smoother*, although it can be used for filtering problems by defining a new smoothing interval at each observational time (e.g. McLaughlin 2002, Reichle 2008, Liu & Gupta 2007).

While both the 1D-Var and 3D-Var methods use a constant state covariance matrix, the 4D-Var evolves the covariance matrix implicitly within the assimilation window and is therefore generally more accurate compared to the 1D-Var and 3D-Var methods (Tsuyuki & Miyoshi 2007). The evolution of the covariance matrix is reset for each new assimilation window and the evolution is called implicit because the covariance matrix is never explicitly calculated in the 4D-Var method (e.g. Reichle 2008). To account for model errors explicitly in the 4D-Var method, the model equations must be used as weak constraints in the cost function, although it increases the variables to be estimated considerably compared to the strong constraint (Tsuyuki & Miyoshi 2007).

Variational methods rely on linearized state and observational models and allow for non-Gaussian probability distributions, although for such cases the cost function may have multiple local minimum solutions (i.e. modes), so more than one solution might be necessary to give sufficient description of the updated probability distribution to find an optimal estimate (Wikle & Berliner 2007). Although the covariance of the optimal estimate can theoretically be obtained from the Hessian of the cost function (e.g. Lewis et al. 2006), it is not provided in variational algorithms (Tsuyuki & Miyoshi 2007) making it generally difficult to provide uncertainty measures for the state estimates for variational data assimilation methods (Wikle & Berliner 2007).

In the remainder of this chapter, the assimilation methods used in this study are described. As before the notation of Lewis et al. (2006) is followed. The classical linear Kalman filter is first introduced followed by a discussion about the square root algorithms. At last the ensemble Kalman square root filter is described.

5.2 Linear Kalman filter

As mentioned earlier, when the stochastic dynamical systems given in equations (5.1) and (5.2) are assumed to be linear and Gaussian, a closed form solution of the updating process (i.e. assimilation process) can be obtained. This solution is referred to as the Kalman filter. In its standard form, additional constraints are imposed on the random errors associated with the model and the observation system. These errors (i.e. w_k and v_k in (5.1) and (5.2)) are assumed to be tempo-

rally uncorrelated and unbiased (i.e. white noise), and there is assumed to be no inter-correlation between the model error, the observation error and the error in the initial state (i.e. e_0 in (5.1)).

The requirement of the errors to be described as white noise is a convenient approximation in cases where the time scales of interest in the assimilation problem are many orders of magnitude larger than the random processes involved (Miller 2007). It has also be recognized that proper treatment of bias, both in the observations and the model, is critically important to the success of a data assimilation systems (e.g. Reichle 2008, Moradkhani et al. 2005*b*). If bias is not treated, the estimates produced in the assimilation process will not be the desired best estimates. It can however be a difficult task to eliminate bias from the problem both because observation bias is often hard to estimate, especially from remotely sensed observations, and because hydrologic models are never perfect and their bias can vary both spatially and temporally (Reichle 2008). The assumption of no autocorrelation can also be violated. Snow storage is for example a cumulative quantity with months of autocorrelation time (Slater & Clark 2006), and related model state variables could therefore show high autocorrelation within the simulated interval.

Methods have been developed to account for both the bias and the autocorrelation in Kalman filters. For example Slater & Clark (2006) alleviated the autocorrelation problem by reducing the update of model state proportional to its correlation with the previous state vector. The autocorrelation problem can also be accounted for by augmentation of the state vector (Reichle et al. 2002), although this increases the dimensionality of the problem. Bias, both in the model and the observations, can similarly be treated within the Kalman filter framework by methods such as augmenting the state vector and the observation vector (e.g. Lewis et al. 2006, Drécourt et al. 2006). Some recent application of Kalman filters have included model parameter updates in the assimilation scheme in order to diminish the effects of model bias (Liu & Gupta 2007, Vrugt et al. 2005), a method which accounts for different model error sources more realistically.

In this study however, no attempt is made to account for model bias, and a Kalman framework will be used where the most stringent assumption about the errors, given above, hold. The linear Kalman filter equations will now be intro-

duced under these assumptions.

The assimilating problem can be stated by considering a state $\mathbf{x}_k$ at time k evolving according to the linear model equations, and a set of observations $\mathscr{F} = \{\mathbf{z}_j \mid 1 \leq j \leq k\}$. The goal is then to find an optimal estimate $\widehat{\mathbf{x}}_k$ of $\mathbf{x}_k$ by assimilating the observation $\mathbf{z}_k$. There are two steps to consider in the Kalman filter, the forecast step and the data assimilation step (also called the analysis step). In the forecast step a prior optimal estimate $\widehat{\mathbf{x}}_{k-1}$ at time $k-1$ is advanced forward in time to obtain the forecast $\mathbf{x}_k^f$ at time k. This forecast is then updated to an optimal estimate $\widehat{\mathbf{x}}_k$ by assimilating the observation $\mathbf{z}_k$. The initial optimal estimate is taken to be $\mathbf{x}_0$ in (5.1) (i.e. $\widehat{\mathbf{x}}_0 \equiv \mathbf{x}_0$) and at each time k, the model error covariance matrix, $\mathbf{Q}_k$, and the observation error covariance, $\mathbf{R}_k$, are assumed to be known. When the model equations and the measurement system are linear, the mappings in equations (5.1) and (5.2) can be replaced by their associated matrices $\mathbf{M}_k \in \mathbb{R}^{n\times n}$ and $\mathbf{H}_k \in \mathbb{R}^{m\times n}$, at time k.

To express the assimilation process sequentially, it is assumed that a prior optimal estimate $\widehat{\mathbf{x}}_{k-1}$ and associated covariance $\widehat{\mathbf{P}}_{k-1}$ are available at time $k-1$. The forecast step is then given by

$$\mathbf{x}_k^f = \mathbf{M}_{k-1}\widehat{\mathbf{x}}_{k-1} \tag{5.4}$$

and the forecast error covariance is given by

$$\mathbf{P}_k^f = \mathbf{M}_{k-1}\widehat{\mathbf{P}}_{k-1}\mathbf{M}_{k-1}^{\mathrm{T}} + \mathbf{Q}_k. \tag{5.5}$$

Here, T denotes the transpose operator. The analysis step includes updating the state vector and the error covariance according to

$$\widehat{\mathbf{x}}_k = \mathbf{x}_k^f + \mathbf{K}_k(\mathbf{z}_k - \mathbf{H}_k\mathbf{x}_k^f) \tag{5.6}$$

and

$$\widehat{\mathbf{P}}_k = (\mathbf{I} - \mathbf{K}_k\mathbf{H}_k)\mathbf{P}_k^f \tag{5.7}$$

respectively. The matrix $\mathbf{K}_k \in \mathbb{R}^{n\times m}$ is called the Kalman gain matrix and is given

by

$$\mathbf{K}_k = \mathbf{P}_k^f \mathbf{H}_k^{\mathrm{T}} [\mathbf{H}_k \mathbf{P}_k^f \mathbf{H}_k^{\mathrm{T}} + \mathbf{R}_k]^{-1}. \tag{5.8}$$

The Kalman filter therefore consists of five equations: two forecast equations (5.4) and (5.5), two analysis equations (5.6) and (5.7), and the Kalman gain (5.8).

The estimate $\widehat{\mathbf{x}}_k$ given in (5.6) is an unbiased minimum variance estimate only if all the assumptions stated above hold. If any of the assumptions do not hold, the filter will be sub-optimal and will not give the best estimate. One of the advantages of Kalman filters is the fact that the error covariance matrix $\widehat{\mathbf{P}}_k$ of the optimal estimate is independent of the observations $\mathbf{z}_k$. As can be seen from (5.7) and (5.8), $\widehat{\mathbf{P}}_k$ is dependent only on the known observation error covariance matrix $\mathbf{R}_k$, the measurement system through $\mathbf{H}_k$, and the model through the forecast error covariance $\mathbf{P}_k^f$. It is therefore possible to design a measurement system and analyse how the covariance matrix $\widehat{\mathbf{P}}_k$ evolves with time before taking any measurements. This feature, and the fact that the error covariance matrix can be evolved with time, is unique to Kalman filters. It is however, computationally expensive to evolve the error covariance matrix according to (5.5) and (5.7) and for large state spaces, lack of information about error structures hinders the construction of meaningful error covariance matrices (Reichle 2008).

When the states are updated with Kalman filters, fundamental principles such as conservation of mass, momentum, and energy are violated within the model boundary (Liu & Gupta 2007). This is on the other hand, an indirect way to make corrections to an imperfect model and the advantage of including multiple states in the updating step has been pointed out by Slater & Clark (2006). If only a small portion of the model states is included, it is not synchronised with other parts of the model so the model has to rebalance, which could be avoided by including more states in the updating step. Disadvantages on the other hand are increased dimensionality of the assimilation as well as extended need to ensure that cross covariance of model states are within physical boundaries.

In (5.6) the term $(\mathbf{z}_k - \mathbf{H}_k \mathbf{x}_k^f)$ is called the innovation or the residual, which is the difference between the real observation $\mathbf{z}_k$ and the model counterpart of the observation $\mathbf{H}_k \mathbf{x}_k^f$. If all the assumptions given above hold, the innovation term exhibits certain statistical properties that can be used to assess the ability of the

model to explain the measurements (Reichle 2008). This is done by comparing theoretical values of the mean and covariance of the innovation to real values obtained in the assimilation process.

The analysis step in (5.6) is a linear combination of the model forecast and the observation. The Kalman gain describes how the innovations are transformed into state space and weights their contribution in updating the states (Drécourt et al. 2006). For example if an observation is much more accurate than the model, i.e. $\mathbf{P}_k^f \gg \mathbf{R}_k$, then the gain is close to one and optimal estimate is close to the observation. When the model is much more accurate, the optimal estimate is similarly close to the model forecast because the gain will be close to zero. It is also possible that low correlation between model states and observations (i.e. low $\mathbf{P}_k^f \mathbf{H}_k^{\mathrm{T}}$) results in a small Kalman gain, which underpins the need to use appropriate observations for efficient data assimilation (Liu & Gupta 2007).

5.3 Square root algorithm

The square root algorithm builds on the fact that symmetric positive definite matrices can be factorized into the product of their associated square root matrices. The fact that square root matrix is non-unique results in many different useful square root filters (Tippett et al. 2003). The use of square root algorithms leads to a numerically stable implementations of the Kalman filter, reducing the effects of round-off errors in computations. Square root algorithms also enable a reduced rank factorization, where the matrix can be approximated by lower rank matrix that only shares the largest eigenvalues, thus reducing the dimensionality of the assimilation problem and saving computational time.

When the square root algorithm is applied to the Kalman filter, the goal is to express the symmetric positive definite error covariance matrices as a product of their square root counterparts. The Kalman filter equations are thus expressed with the square root matrices instead of the full error covariance matrices when the square root algorithm is applied.

5.4 Ensemble Kalman square root filter

When the model equations in (5.1) are non-linear, the assimilation problem can no longer be solved by the linear Kalman filter. One way of solving this non-linear problem is to apply the standard Monte Carlo framework by producing an ensemble of possible values for the forecast vector $\mathbf{x}_k^f$ and the optimal estimate $\widehat{\mathbf{x}}_k$, after which sample moments can be used to estimate the resulting forecast, optimal estimate, and associated covariances. This method is utilized in the ensemble Kalman filter.

Except for linearity, the same assumptions apply to the ensemble Kalman filter in its standard form as for the linear Kalman filter. That is, the model error and the observation error are assumed to be white Gaussian noise with covariance matrices $\mathbf{Q}_k$ and $\mathbf{R}_k$ respectively. It is also assumed that no inter-correlation exists between the model error, the observation error, and the error of the initial condition.

The equations that make up the ensemble Kalman square root filter will now be stated with the notation from Lewis et al. (2006). Instead of one update (i.e. involving the Kalman gain) equation for the linear Kalman filter, there are two updating equations for the ensemble Kalman square root filter. The mean and the anomalies are updated separetly as will be shown below.

To express the updating process sequencially it is assumed that at a time $k-1$, there exist an optimal estimate for N ensemble members, $\widehat{\xi}_{k-1}(i)$ for $i = 1,\ldots,N$, and associated covariance matrix $\widehat{\mathbf{P}}_{k-1}(N)$. This optimal estimate is advanced forward in time by applying the non-linear model equations according to

$$\xi_k^f(i) = \mathbf{M}\big(\widehat{\xi}_{k-1}(i)\big), \tag{5.9}$$

to give the forecast ensemble. The sample mean, given by

$$\mathbf{x}_k^f(N) = \frac{1}{N}\sum_{i=1}^{N} \xi_k^f(i), \tag{5.10}$$

is therefore representative of the expected forecast. The covariance of this forecast

ensemble is given by

$$\begin{aligned}\mathbf{P}_k^f(N) &= \frac{1}{N-1}\sum_{i=1}^{N}\left[\xi_k^f(i)-\mathbf{x}_k^f(N)\right]\left[\xi_k^f(i)-\mathbf{x}_k^f(N)\right]^{\mathrm{T}} \\ &= \frac{1}{N-1}\sum_{i=1}^{N}\mathbf{e}_k^f(i)\left(\mathbf{e}_k^f(i)\right)^{\mathrm{T}}, \end{aligned} \tag{5.11}$$

where the forecast anomaly term $\mathbf{e}_k^f(i)$ is given by

$$\mathbf{e}_k^f(i) = \xi_k^f(i) - \mathbf{x}_k^f(N). \tag{5.12}$$

The two update equations are now given by

$$\begin{aligned}\widehat{\mathbf{x}}_k(N) &= \frac{1}{N}\sum_{i=1}^{N}\widehat{\xi}_k(i) \\ &= \mathbf{x}_k^f(N) + \mathbf{K}_k\left[z_k - \mathbf{H}_k\mathbf{x}_k^f(N)\right] \end{aligned} \tag{5.13}$$

and

$$\widehat{\mathbf{e}}_k(i) = \mathbf{e}_k^f(i) + \mathbf{W}_k\mathbf{H}_k\mathbf{e}_k^f(i), \tag{5.14}$$

where the anomaly term for the optimal estimate is given by

$$\widehat{\mathbf{e}}_k(i) = \widehat{\xi}_k(i) - \widehat{\mathbf{x}}_k(N). \tag{5.15}$$

The matrices $\mathbf{K}_k$ in (5.13) and $\mathbf{W}_k$ in (5.14) are called the Kalman gain and the *modified* Kalman gain respectively and $\mathbf{z}_k$ is, as before, an observation at a time k. The form of the Kalman gain is the same as for the linear Kalman filter, except the sample covariance is used here according to

$$\mathbf{K}_k = \mathbf{P}_k^f(N)\mathbf{H}_k^{\mathrm{T}}[\mathbf{H}_k\mathbf{P}_k^f(N)\mathbf{H}_k^{\mathrm{T}} + \mathbf{R}_k]^{-1}. \tag{5.16}$$

The *modified* Kalman gain is given by

$$\mathbf{W}_k = \mathbf{P}_k^f(N)\mathbf{H}_k^{\mathrm{T}}\mathbf{S}^{-\mathrm{T}}(\mathbf{S}+\mathbf{F})^{-1}, \tag{5.17}$$

with the square root factors $\mathbf{S}$ and $\mathbf{F}$ given by

$$\mathbf{S}\mathbf{S}^{\mathrm{T}} = \mathbf{H}_k \mathbf{P}_k^f(N)\mathbf{H}_k^{\mathrm{T}} + \mathbf{R}_k \qquad \text{and} \qquad \mathbf{F}\mathbf{F}^{\mathrm{T}} = \mathbf{R}_k \tag{5.18}$$

respectively. Finally, the covariance matrix for the optimal estimate is given by

$$\widehat{\mathbf{P}}_k(N) = \frac{1}{N-1}\sum_{i=1}^{N} \widehat{\mathbf{e}}_k(i)\big(\widehat{\mathbf{e}}_k(i)\big)^{\mathrm{T}}. \tag{5.19}$$

The equations described above are needed in the ensamble Kalman square root filter.

In this study, 100 ensemble members were generated and remotely sensed snow covered area assimilated into the model by use of the ensemble Kalman square root filter. Two states were updated, the total snow accumulation state variable, μ, and the total snow melt state variable, D_m. A cloud cover threshold of 25 % was used, i.e. no observations were used if the cloud cover exceeded 25 %. After each assimilation cycle, the snow covered area, SCA, and the snow water equivalent, SWE, were updated through Equations (4.4d) and (4.4e) (p. 22) respectively, based on the new updated values for μ and D_m.

6 Evaluation

The highest sub-basin in the Jollie Catchment (see Figure 3.2, p. 13) is selected for analysis. Subsequently, all figures presented in this chapter are based on data from this sub-basin.

The forcing data (i.e. input data) have already been presented in Chapter 3.1 (p. 9), where the precipitation is perturbed to create ensemble of model trajectories. This ensemble, representing the model error or uncertainty, is then used in the ensemble Kalman square root filter to update model states based on remotely sensed snow covered area information. As the model is not calibrated in this study (i.e. default model parameters are used, see Table 4.1, p. 19), two withholding experiments were conducted, where snow covered area observations are withheld during assimilation process. In the first withholding experiment, all snow covered area observations from the sub-basin were omitted in the assimilation process (i.e. spatial withholding experiment), and in the second one, every second observation was used (i.e. temporal withholding experiment). By comparing the resulting updated ensemble of simulated snow covered area with the withheld observations, gives a quantitative measure of the assimilation performance. A purely visual method will be applied in assessing the impacts that the assimilation process has on the model state variables. This will be achieved by comparing time series of updated versus non-updated states graphically.

6.1 Correlation

Correlation between simulated snow covered area, SCA, and other state variables gives a clue of how effective the assimilation process is going to be. If there is no correlation at all, it results in zero Kalman gain, which means that no model states will be affected by the assimilation process.

Figure 6.1 shows how SCA is correlated to the snow water equivalent, SWE, the total snow accumulation, μ, and the total snow melt, D_m, within the highest sub-basin. This shows a good correlations between SCA and SWE during the ablation season (i.e. > 0.7 from September) but poor correlation during the winter months. The total snow accumulation state, μ, is poorly correlated with SCA for most

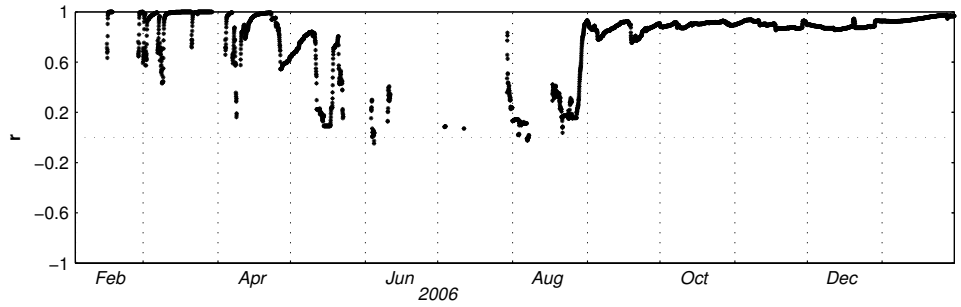

(a) Correlation between snow covered area, SCA, and snow water equivalent, SWE.

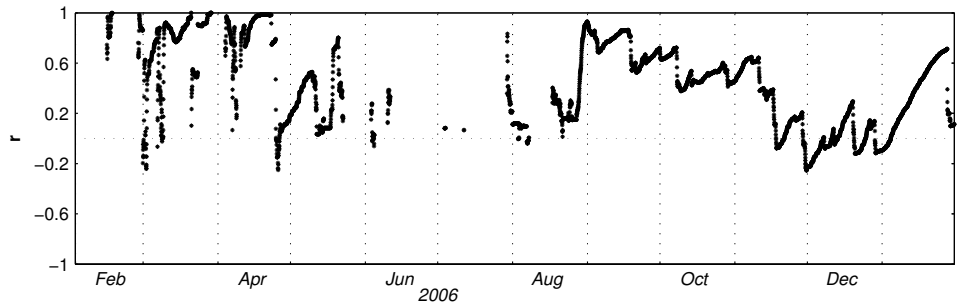

(b) Correlation between snow covered area, SCA, and total accumulation state variable, μ.

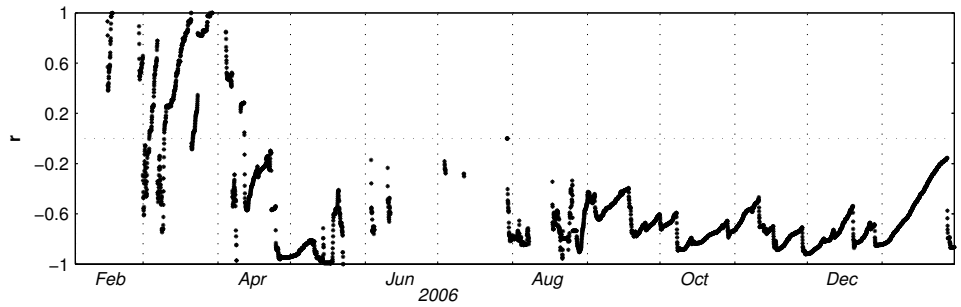

(c) Correlation between snow covered area, SCA, and total melt state variable, D_m.

Figure 6.1: Correlation between fractional snow covered area and three other state variables.

of the ablation season except in the first two weeks of September. Total snow melt snow considerably better correlation, compared to total accumulation, and is below -0.6 for a good part of the ablation period. Pre-winter correlations between SCA and total accumulation and the melt states (μ and D_m) tend to be much more fluctuating and only show strong correlations for short time periods.

6.2 Impacts of assimilation

As the total snow melt and total snow accumulation were the only states that were directly updated in the assimilation process, their correlation with the simulated snow covered area is one of the controlling factor of how effective the assimilation will be. As seen in Figure 6.1, the strongest correlations occurred during the ablation period. It is therefore not surprising that the assimilation has strong im-

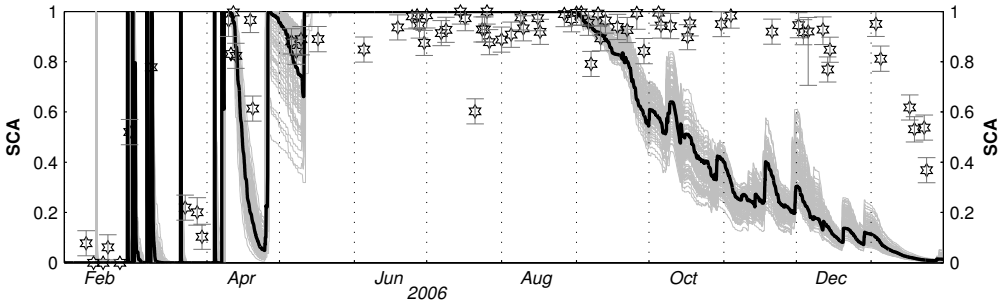

(a) Simulated snow covered area, SCA, *before* assimilation of snow covered area observations.

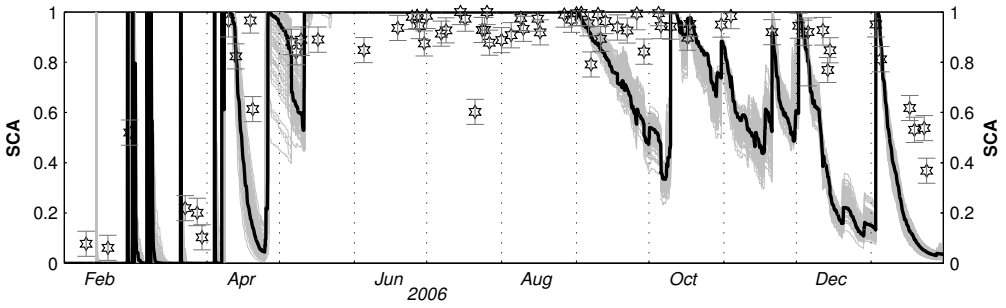

(b) Simulated snow covered area, SCA, *after* assimilation of snow covered area observations.

Figure 6.2: Comparison between simulated snow covered area, SCA, *before* and *after* assimilation of snow covered area observations. Remotely sensed snow covered area observations and associated error estimates are also shown.

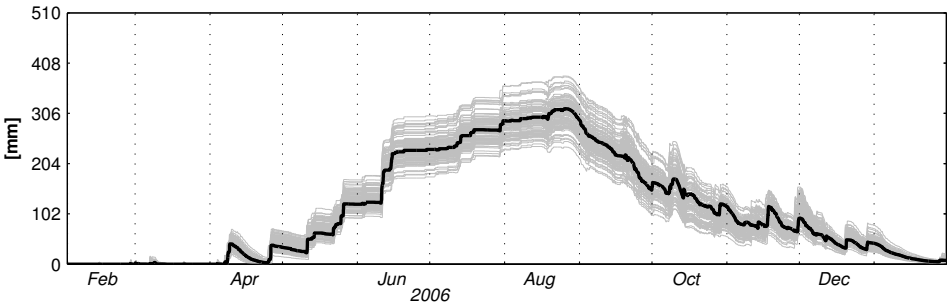

(a) Snow water equivalent, SWE, *before* assimilation of snow covered area observations.

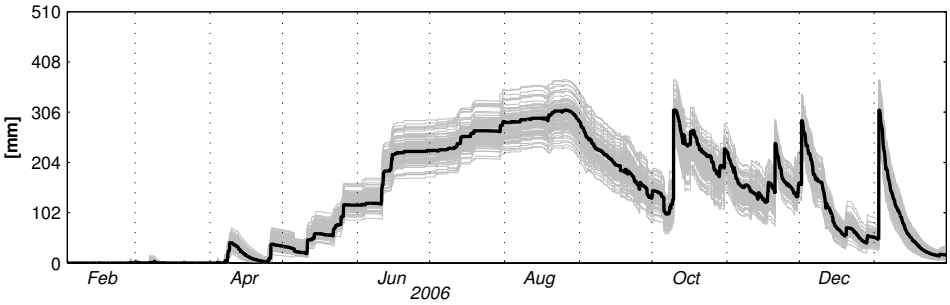

(b) Snow water equivalent, SWE, *after* assimilation of snow covered area observations.

Figure 6.3: Comparison between snow water equivalent, SWE, *before* and *after* assimilation of snow covered area observations.

pact during the ablation, from October onwards according to Figures 6.2 and 6.3, but negligible effects at other times. By examining Fiure 6.2 it is evident that the assimilation process reduces SCA during September and beginning of October, although the observed SCA for this sub-basin all indicate that SCA should be higher. This is most likely due to information propagated from other sub-basins showing lower SCA. After early October, the updated SCA is very close to observations and suggest that the model is missing snowfall events in the ablation season or underestimating snow storage in the end of winter.

6.3 Withholding experiments

The idea with the withholding experiments is to compare the assimilation results with independent measurements. Two withholding experiments were conducted. Spatial withholding experiment, in which all observations for the sub-basin were withheld, and temporal withholding experiment, in which every second observation was withheld (compare Figure 6.2(a), p. 41, with Figure 6.4). These experiments show good agreement between observations and model simulation of snow covered area. Moreover, the simulated snow covered area in the sub-basin is not affected by withholding observations in it, which indicates that information from other sub-basins contribute strongly to the updating process within this sub-basin.

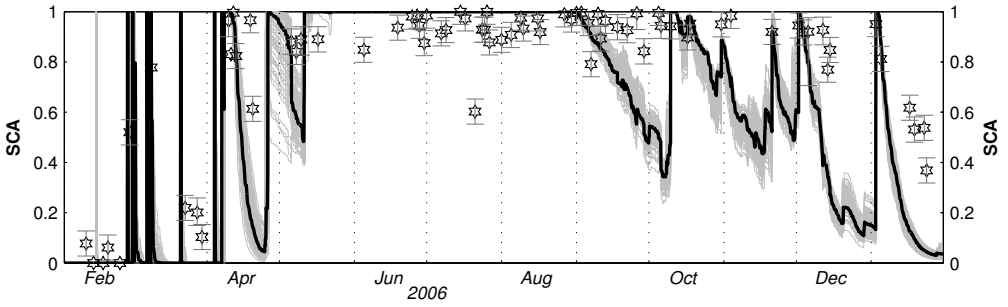

(a) Simulated snow covered area, SCA, *after* assimilation of snow covered area observations in a spatial withholding experiment.

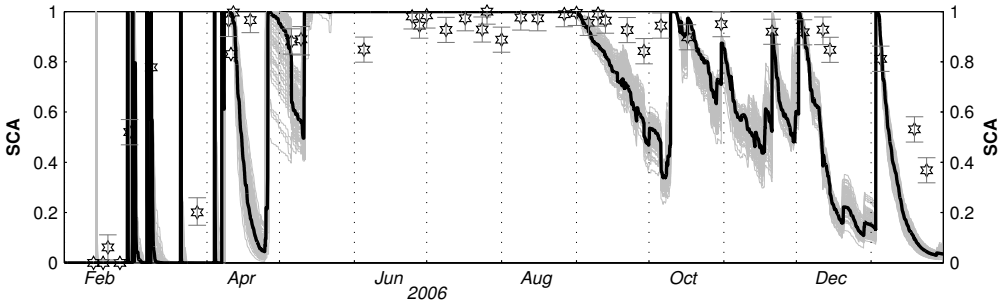

(b) Simulated snow covered area, SCA, *after* assimilation of snow covered area observation in a temporal withholding experiment.

Figure 6.4: Comparison between simulated snow covered area, SCA, *after* assimilation of snow covered area observation in a spatial and temporal withholding experiment. The withheld snow covered area observations (i.e. the ones not used in the assimilation process) are also shown.

7 Concluding remarks

In this study, a remotely sensed snow covered area was assimilated into a hydrologic model, using the ensemble Kalman square root filter. The assimilation was effective only during the ablation season, when strong correlation existed between simulated snow covered area and the state variables that were updated in the assimilation process, which were the total snow accumulation and the total snow melt. According to the assimilation results for the highest sub-basin in the Jollie Catchment, the model underestimates end of winter snow storage and/or it does not pick up occasional snow falls in the ablation season. Two withholding experiments showed that the assimilation fits the observations resonably well and withholding observations from the highest sub-basin does not affect the resulting updated simulated snow covered area, which means that information from other sub-basins strongly contribute to the update.

This study shows that remotely sensed snow covered information is a valuable sorce of data that has a potential to be useful in hydrologic modelling for New Zealand conditions. Thus, using an assimilation scheme to incorporate remotely sensed data into models is a good way to improve the ability of the model to represent nature.

Suggestions for future studies might be to use measured snow water equivalent to validate and/or calibrate the model to obtain more realistic model simulations and therefore more efficient assimilation. This might also be acomplished by calibrating the model with respect to measured runoff. In this study, only one highest sub-basin in the Jollie Catchment was examining. Further work might include examine the impacts of assimilation for other sub-basins within the Jollie Catchment, looking at different model grid resolutions, or extending the study area within the limits of available remotely sensed data.

References

Abramowitz, G., Gupta, H., Pitman, A., Wang, Y., Leuning, R., Cleugh, H. & Hsu, K.-l. (2006), 'Neural Error Regression Diagnosis (NERD): A tool for model bias identification and prognostic data assimilation', *Journal of Hydrometeorology* **7**(1), 160–177.

Anderton, S. P., White, S. M. & Alvera, B. (2004), 'Evaluation of spatial variability in snow water equivalent for a high mountain catchment', *Hydrological Processes* **18**(3), 435–453.

Andreadis, K. M. & Lettenmaier, D. P. (2006), 'Assimilating remotely sensed snow observations into a macroscale hydrology model', *Advances in Water Resources* **29**(6), 872–886.

Balk, B. & Elder, K. (2000), 'Combining binary decision tree and geostatistical methods to estimate snow distribution in a mountain watershed', *Water Resources Research* **36**(1), 13–26.

Bandaragoda, C., Tarboton, D. G. & Woods, R. (2004), 'Application of TOPNET in the distributed model intercomparison project', *Journal of Hydrology* **298**(1-4), 178–201.

Barringer, J. R. F., Pairman, D. & McNeill, S. J. (2002), Development of a high-resolution digital elevation model for New Zealand, Contract Report LC0102/170, Landcare Research, Lincoln, New Zealand.

Bird, R. E. & Riordan, C. (1986), 'Simple solar spectral model for direct and diffuse irradiance on horizontal and tilted planes at the earth's surface for cloudless atmospheres.', *Journal of Climate & Applied Meteorology* **25**(1), 87–97.

Blöschl, G. (1999), 'Scaling issues in snow hydrology', *Hydrological Processes* **13**(14-15), 2149–2175.

Clark, M. P., Ibbitt, R. P. & Woods, R. A. (2007), 'Flood forecasts for New Zealand communities', *Water & Atmosphere* **15**(3), 14–15.

Clark, M. P., Rupp, D. E., Woods, R. A., Zheng, X., Ibbitt, R. P., Slater, A. G., Schmidt, J. & Uddstrom, M. J. (2008), 'Hydrological data assimilation with the ensemble Kalman filter: use of streamflow observations to update states in a distributed hydrological model', *Advances in Water Resources* . In Press.

Clark, M. P. & Slater, A. G. (2006), 'Probabilistic quantitative precipitation estimation in complex terrrain', *Journal of Hydrometeorology* **7**(1), 3–22.

Clark, M. P., Slater, A. G., Barrett, A. P., Hay, L. E., McCabe, G. J., Rajagopalan, B. & Leavesley, G. H. (2006), 'Assimilation of snow covered area information into hydrologic and land-surface models', *Advances in Water Resources* **29**(8), 1209–1221.

Derksen, C. P., Walker, A. E. & Goodison, B. E. (2003), 'A comparison of 18 winter seasons of in situ and passive microwave-derived snow water equivalent estimates in Western Canada', *Remote Sensing of Environment* **88**(3), 271–282.

Déry, S. J., Salomonson, V. V., Stieglitz, M., Hall, D. K. & Appel, I. (2005), 'An approach to using snow areal depletion curves inferred from MODIS and its application to land surface modelling in Alaska', *Hydrological Processes* **19**(14), 2755–2774.

Dong, J., Walker, J. P., Houser, P. R. & Sun, C. (2007), 'Scanning multichannel microwave radiometer snow water equivalent assimilation', *Journal of Geophysical Research D: Atmospheres* **112**(7), D07108 1–16.

Dressler, K. A., Leavesley, G. H., Bales, R. C. & Fassnacht, S. R. (2006), 'Evaluation of gridded snow water equivalent and satellite snow cover products for mountain basins in a hydrologic model', *Hydrological Processes* **20**(4), 673–688.

Drécourt, J.-P., Madsen, H. & Rosbjerg, D. (2006), 'Bias aware Kalman filters: Comparison and improvements', *Advances in Water Resources* **29**(5), 707–718.

Dunne, S. & Entekhabi, D. (2005), 'An ensemble-based reanalysis approach to land data assimilation', *Water Resources Research* **41**(2), W02013 1–18.

Ehrendorfer, M. (2007), 'A review of issues in ensemble-based Kalman filtering', *Meteorologische Zeitschrift* **16**(6), 795–818.

Elder, K., Rosenthal, W. & Davis, R. E. (1998), 'Estimating the spatial distribution of snow water equivalence in a montane watershed', *Hydrological Processes* **12**(10-11), 1793–1808.

Erxleben, J., Elder, K. & Davis, R. (2002), 'Comparison of spatial interpolation methods for estimating snow distribution in the Colorado Rocky Mountains', *Hydrological Processes* **16**(18), 3627–3649.

Evensen, G. (1994), 'Sequential data assimilation with a nonlinear quasi-geostrophic model using monte carlo methods to forecast error statistics', *Journal of Geophysical Research* **99**(C5), 10,143–10,162.

Fassnacht, S. R. (2007), 'Data time step to estimate snowpack accumulation at select united states meteorological stations', *Hydrological Processes* **21**(12), 1608–1615.

Fitzharris, B. B. (1979), Snow hydrology, *in* D. L. Murray & P. Ackroyd, eds, 'Physical hydrology – New Zealand experience', New Zealand Hydrological Society, Wellington, pp. 23–43.

Fitzharris, B. B. (1987), A method for indexing the variability of alpine seasonal snow over large areas, *in* B. E. Goodinson, R. G. Barry & J. Dozier, eds, 'Large scale effects of seasonal snow cover', number 166 *in* 'IAHS Publications', IAHS, IAHS Press, Wallingford, Oxfordshire, UK, pp. 139–150.

Fitzharris, B. B. (1992), 'The electricity crisis and the role of climate and hydrology', *New Zealand Geographer* **48**(2), 79–83.

Fitzharris, B. B. & Garr, C. E. (1995), 'Simulation of past variability in seasonal snow in the Southern Alps, New Zealand', *Annals of Glaciology* **21**, 377–382.

Fitzharris, B. B. & Grimmond, C. S. B. (1982), Assessing snow storage and melt in a New Zealand mountain environment., *in* J. W. Glen, ed., 'Hydrological Aspects of Alpine and High-Mountain Areas', number 138 *in* 'IAHS Publications', IAHS, IAHS Press, Wallingford, Oxfordshire, UK, pp. 161–168.

Fitzharris, B. B., Lawson, W. J. & Owens, I. F. (1999), 'Research on glaciers and snow in New Zealand', *Progress in Physical Geography* **23**(4), 469–500.

Flanner, M. G. & Zender, C. S. (2006), 'Linking snowpack microphysics and albedo evolution', *Journal of Geophysical Research D: Atmospheres* **111**(12), D12208 1–12.

Ghanbarpour, M. R., Saghafian, B., Saravi, M. M. & Abbaspour, K. C. (2007), 'Evaluation of spatial and temporal variability of snow cover in a large mountainous basin in Iran', *Nordic Hydrology* **38**(1), 45–58.

Hall, D. K. & Riggs, G. A. (2007), 'Accuracy assessment of the MODIS snow products', *Hydrological Processes* **21**(12), 1534–1547.

Hall, D. K., Riggs, G. A. & Salomonson, V. V. (1995), 'Development of methods for mapping global snow cover using moderate resolution imaging spectroradiometer data', *Remote Sensing of Environment* **54**(2), 127–140.

Hall, D. K., Riggs, G. A., Salomonson, V. V., DiGirolamo, N. E. & Bayr, K. J. (2002), 'MODIS snow-cover products', *Remote Sensing of Environment* **83**(1-2), 181–194.

Hartman, M. D., Baron, J. S., Lammers, R. B., Cline, D. W., Band, L. E., Liston, G. E. & Tague, C. (1999), 'Simulations of snow distribution and hydrology in a mountain basin', *Water Resources Research* **35**(5), 1587–1603.

Henderson, R. D. & Thompson, S. M. (1999), 'Extreme rainfalls in the Southern Alps of New Zealand', *Journal of Hydrology New Zealand* **38**(2), 309–330.

Keshava, N. (2003), 'A survey of spectral unmixing algorithms', *Lincoln Laboratory Journal* **14**(1), 55–78.

Kolberg, S. A. & Gottschalk, L. (2006), 'Updating of snow depletion curve with remote sensing data', *Hydrological Processes* **20**(11), 2363–2380.

Kolberg, S., Rue, H. & Gottschalk, L. (2006), 'A Bayesian spatial assimilation scheme for snow coverage observations in a gridded snow model', *Hydrology and Earth System Sciences* **10**(3), 369–381.

Kumar, S. V., Reichle, R. H., Peters-Lidard, C. D., Koster, R. D., Zhan, X., Crow, W. T., Eylander, J. B. & Houser, P. R. (2008), A land surface data assimilation framework using the land information system: Description and applications. In Press.

Lewis, J. M., Lakshmivarahan, S. & Dhall, S. K. (2006), *Dynamic data assimilation : a least squares approach*, Cambridge University Press, Cambridge.

Liston, G. E. (1999), 'Interrelationships among snow distribution, snowmelt, and snow cover depletion: Implications for atmospheric, hydrologic, and ecologic modeling', *Journal of Applied Meteorology* **38**(10), 1474–1487.

Liston, G. E. (2004), 'Representing subgrid snow cover heterogeneities in regional and global models', *Journal of Climate* **17**(6), 1381–1397.

Liu, Y. & Gupta, H. V. (2007), 'Uncertainty in hydrologic modeling: Toward an integrated data assimilation framework', *Water Resources Research* **43**(7), W07401 1–18.

Luce, C. H. & Tarboton, D. G. (2004), 'The application of depletion curves for parameterization of subgrid variability of snow', *Hydrological Processes* **18**(8), 1409–1422.

Luce, C. H., Tarboton, D. G. & Cooley, K. R. (1999), 'Sub-grid parameterization of snow distribution for an energy and mass balance snow cover model', *Hydrological Processes* **13**(12-13), 1921–1933.

Mathieu, P.-P. & O'Neill, A. (2008), 'Data assimilation: From photon counts to Earth System forecasts', *Remote Sensing of Environment* **112**(4), 1258–1267.

McGuire, M., Wood, A. W., Hamlet, A. F. & Lettenmaier, D. P. (2006), 'Use of satellite data for streamflow and reservoir storage forecasts in the Snake River Basin', *Journal of Water Resources Planning and Management* **132**(2), 97–110.

McLaughlin, D. B. (2002), 'An integrated approach to hydrologic data assimilation: Interpolation, smoothing, and filtering', *Advances in Water Resources* **25**(8-12), 1275–1286.

Miller, R. N. (2007), 'Topics in data assimilation: Stochastic processes', *Physica D: Nonlinear Phenomena* **230**(1-2), 17–26.

Miller, R. N., Ghil, M. & Gauthiez, F. (1994), 'Advanced data assimilation in strongly nonlinear dynamical systems', *Journal of the Atmospheric Sciences* **51**(8), 1037–1056.

Moradkhani, H., Hsu, K.-L., Gupta, H. V. & Sorooshian, S. (2005*a*), 'Uncertainty assessment of hydrologic model states and parameters: Sequential data assimilation using the particle filter', *Water Resources Research* **41**(5), W05012 1–17.

Moradkhani, H., Sorooshian, S., Gupta, H. V. & Houser, P. R. (2005*b*), 'Dual state-parameter estimation of hydrological models using ensemble kalman filter', *Advances in Water Resources* **28**(2), 135–147.

New Zealand Meteorological Service (1985), *Part 6, Annual rainfall*, number 175 *in* 'New Zealand Meteorlogical Service Miscellaneous Publication', Ministry of Transport New Zealand Meteorological Service, Wellington, New Zealand.

Norton, D. A. (1985), 'A multivariate technique for estimating New Zealand temperature normals', *Weather and Climate* **5**(2), 64–74.

Pulliainen, J. (2006), 'Mapping of snow water equivalent and snow depth in boreal and sub-arctic zones by assimilating space-borne microwave radiometer data and ground-based observations', *Remote Sensing of Environment* **101**(2), 257–269.

Reichle, R. H. (2008), Data assimilation methods in the Earth sciences. In Press.

Reichle, R. H., McLaughlin, D. B. & Entekhabi, D. (2002), 'Hydrologic data assimilation with the ensemble Kalman filter', *Monthly Weather Review* **130**(1), 103–114.

Richter, R. (1998), 'Correction of satellite imagery over mountainous terrain', *Applied Optics* **37**(18), 4004–4015.

Rupp, D. E., Keim, R. F., Ossiander, M., Brugnach, M. & Selker, J. S. (2006), Temporal rainfall disaggregation by multiplicative cascades conditioned on timescale, intensity, and position within sequence. Unpublished.

Salomonson, V. V. & Appel, I. (2004), 'Estimating fractional snow cover from MODIS using the normalized difference snow index', *Remote Sensing of Environment* **89**(3), 351–360.

Schaper, J., Martinec, J. & Seidel, K. (1999), 'Distributed mapping of snow and glaciers for improved runoff modelling', *Hydrological Processes* **13**(12-13), 2023–2031.

Sirguey, J. P. (2008), MODIS-derived maps of subpixel snow fraction: Data description. Unpublished.

Sirguey, J. P., Mathieu, R., Arnaud, Y., Khanand, M. M. & Chanussot, J. (2008), 'Improving MODIS spatial resolution for snow mapping using wavelet fusion and ARSIS concept', *IEEE Geoscience and Remote Sensing Letters* **5**(1), 78–82.

Skaugen, T., Beldring, S. & Udnæs, H.-C. (2003), 'Dynamical properties of the spatial distribution of snow', *Hydrology and Earth System Sciences* **7**(5), 744–753.

Slater, A. G. & Clark, M. P. (2006), 'Snow data assimilation via an ensemble Kalman filter', *Journal of Hydrometeorology* **7**(3), 478–493.

Snelder, T. H. & Biggs, B. J. F. (2002), 'Multiscale river environment classification for water resources management', *Journal of the American Water Resources Association* **38**(5), 1225–1239.

Sturman, A. P., McGowan, H. A. & Spronken-Smith, R. A. (1999), 'Mesoscale and local climates in New Zealand', *Progress in Physical Geography* **23**(4), 611–635.

Tait, A., Henderson, R., Turner, R. & Zheng, X. (2006), 'Thin plate smoothing spline interpolation of daily rainfall for New Zealand using a climatological rainfall surface', *International Journal of Climatology* **26**(14), 2097–2115.

Tait, A. & Zheng, X. (2007), 'Analysis of the spatial interpolation error associated with maps of median annual climate variables', On-line publication.
URL: *http://www.niwa.cri.nz/__data/assets/pdf_file/0006/52557/Climate_Maps_Error_Analysis.pdf*

Tekeli, A. E., Akyürek, Z., Şorman, A. A., Şensoy, A. & Şorman, A. Ü. (2005), 'Using MODIS snow cover maps in modeling snowmelt runoff process in the eastern part of Turkey', *Remote Sensing of Environment* **97**(2), 216–230.

Terralink International Limited (2004), 'New Zealand Land Cover Database (LCDB2)', NZ Climate Office, Ministry for the Environment.

Tippett, M. K., Anderson, J. L., Bishop, C. H., Hamill, T. M. & Whitaker, J. S. (2003), 'Ensemble square root filters', *Monthly Weather Review* **131**(7), 1485–1490.

Tsuyuki, T. & Miyoshi, T. (2007), 'Recent progress of data assimilation methods in meteorology', *Journal of the Meteorological Society of Japan* **85 B**, 331–361.

Turcotte, R., Fortin, L.-G., Fortin, V., Fortin, J.-P. & Villeneuve, J.-P. (2007), 'Operational analysis of the spatial distribution and the temporal evolution of the snowpack water equivalent in southern Québec, Canada', *Nordic Hydrology* **38**(3), 211–234.

Turner, M. R. J., Walker, J. P. & Oke, P. R. (2008), 'Ensemble member generation for sequential data assimilation', *Remote Sensing of Environment* **112**(4), 1421–1433.

Udnæs, H.-C., Alfnes, E. & Andreassen, L. M. (2007), 'Improving runoff modelling using satellite-derived snow covered area?', *Nordic Hydrology* **38**(1), 21–32.

Vrugt, J. A., Diks, C. G. H., Gupta, H. V., Bouten, W. & Verstraten, J. M. (2005), 'Improved treatment of uncertainty in hydrologic modeling: Combining the strengths of global optimization and data assimilation', *Water Resources Research* **41**(1), W01017 1–17.

Wikle, C. K. & Berliner, L. M. (2007), 'A Bayesian tutorial for data assimilation', *Physica D: Nonlinear Phenomena* **230**(1-2), 1–16.

Yang, D., Robinson, D., Zhao, Y., Estilow, T. & Ye, B. (2003), 'Streamflow response to seasonal snow cover extent changes in large Siberian watersheds', *Journal of Geophysical Research D: Atmospheres* **108**(D18), 4578 ACL–7 1–14.